Geophysical Journal International

Geophys. J. Int. (2015) **202,** 1392–1406
GJI Gravity, geodesy and tides

doi: 10.1093/gji/ggv227

A normal mode treatment of semi-diurnal body tides on an aspherical, rotating and anelastic Earth

Harriet C.P. Lau,[1] Hsin-Ying Yang,[2,3] Jeroen Tromp,[2] Jerry X. Mitrovica,[1] Konstantin Latychev[4] and David Al-Attar[5]

[1]*Department of Earth and Planetary Sciences, Harvard University, MA* 02143, *USA. E-mail: harrietlau@fas.harvard.edu*
[2]*Department of Geosciences and Program in Applied & Computational Mathematics, Princeton University, NJ* 08544, *USA*
[3]*Department of Geosciences, National Taiwan University, Taipei, Taiwan*
[4]*Department of Physics, University of Toronto, Toronto, Ontario* M5S 1A7, *Canada*
[5]*Bullard Laboratories, Department of Earth Sciences, University of Cambridge, Cambridge, United Kingdom*

Accepted 2015 May 28. Received 2015 May 27; in original form 2014 October 8

SUMMARY

Normal mode treatments of the Earth's body tide response were developed in the 1980s to account for the effects of Earth rotation, ellipticity, anelasticity and resonant excitation within the diurnal band. Recent space-geodetic measurements of the Earth's crustal displacement in response to luni-solar tidal forcings have revealed geographical variations that are indicative of aspherical deep mantle structure, thus providing a novel data set for constraining deep mantle elastic and density structure. In light of this, we make use of advances in seismic free oscillation literature to develop a new, generalized normal mode theory for the tidal response within the semi-diurnal and long-period tidal band. Our theory involves a perturbation method that permits an efficient calculation of the impact of aspherical structure on the tidal response. In addition, we introduce a normal mode treatment of anelasticity that is distinct from both earlier work in body tides and the approach adopted in free oscillation seismology. We present several simple numerical applications of the new theory. First, we compute the tidal response of a spherically symmetric, non-rotating, elastic and isotropic Earth model and demonstrate that our predictions match those based on standard Love number theory. Second, we compute perturbations to this response associated with mantle anelasticity and demonstrate that the usual set of seismic modes adopted for this purpose must be augmented by a family of relaxation modes to accurately capture the full effect of anelasticity on the body tide response. Finally, we explore aspherical effects including rotation and we benchmark results from several illustrative case studies of aspherical Earth structure against independent finite-volume numerical calculations of the semi-diurnal body tide response. These tests confirm the accuracy of the normal mode methodology to at least the level of numerical error in the finite-volume predictions. They also demonstrate that full coupling of normal modes, rather than group coupling, is necessary for accurate predictions of the body tide response.

Key words: Tomography; Tides and planetary waves; Surface waves and free oscillations; Theoretical seismology.

1 INTRODUCTION

Predicting deformation of the solid Earth in response to periodic luni-solar forcings, the so-called body tides, has a rich history in classical geophysics. Early theoretical studies considered the response of a homogeneous, incompressible, elastic sphere (Thomson 1863), and also derived a set of dimensionless numbers, the so-called Love and/or Shida numbers, that map the tidal forcing into radial and horizontal crustal displacements and perturbations in the geopotential (Love 1911; Shida 1912). Later studies in the second half of the 20th century incorporated spherically symmetric elastic and density structure, including an inviscid core, into the theoretical and numerical treatment of Love numbers (Takeuchi 1950; Alterman *et al.* 1959; Farrell 1972) and also accounted for the effects of rotation and ellipticity (Wahr 1981a,b), anelasticity and resonances in the diurnal band associated with the free-core nutation (Wahr & Bergen 1986), and excess ellipticity (Dehant *et al.* 1999). Most recently, finite element/volume numerical schemes have been described that compute the body tide response of Earth models with 3-D variations in elastic and density structure (Métivier & Conrad 2008; Latychev *et al.* 2009).

Initially, body tide research was largely dedicated to making predictions with sufficient accuracy that their effect on observations of the Earth's solid surface and gravitational field could be removed, thus isolating other signals for investigation. Indeed, corrections of this kind are now routinely incorporated into most GPS analysis standards (e.g. Petit & Luzum 2010). To this end, the series of canonical papers by Wahr and colleagues (Wahr 1981a,b; Wahr & Bergen 1986) directly linked the Earth's body tides to an eigenfunction expansion developed within normal mode (or free oscillation) seismology. In this paper, we revisit the normal mode treatment of the tidal problem for three reasons: (i) to update the theory by taking advantage of important advances in free oscillation theory, namely a perturbation approach for incorporating aspherical (i.e. 3-D or laterally heterogeneous) Earth structure; (ii) to include a rigorous method for dealing with the non-Hermitian operator that arises when considering rotating and anelastic Earth models (Lognonné 1991); and (iii) to introduce a treatment of anelasticity that is more general than the approach introduced in previous work (Wahr & Bergen 1986).

Our effort is motivated by progressive improvements in the accuracy of space-geodetic measurements, which has now reached a level where these additional complexities have become relevant to the analysis of the body tide response (e.g. Herring & Dong 1994; Mitrovica *et al.* 1994; Yuan & Chao 2012; Krásná *et al.* 2013). Moreover, such improvements provide a novel means to investigate the internal structure of the Earth. Of particular relevance in this regard are the three recent studies of Ito & Simons (2011), Yuan *et al.* (2013) and Qin *et al.* (2014). Ito & Simons (2011) used regional variability in the ocean tidal loading displacement across the western USA, as measured by GPS using the Plate Boundary Observatory network, to estimate subsurface elastic and density structure. Furthermore, motivated by the GRAIL satellite gravity mission, Qin *et al.* (2014) derived a normal mode perturbation theory to predict the impact of laterally heterogeneous elastic structure on lunar body tides and (ultimately) to infer long wavelength internal structure of the Moon, which is thought to be dominated by nearside–farside heterogeneity. Finally, Yuan *et al.* (2013) used a global GPS network to estimate geographical variations of the Earth's semi-diurnal and diurnal body tide displacements with submillimetre precision. These variations are likely indicative of aspherical Earth structure.

Our aim here is to derive a complete theory for predicting semi-diurnal body tides on an aspherical, rotating and anelastic Earth, and to describe a practical framework for accurately implementing the theory. The theory can accommodate long-period tides but it does not extend to the prediction of the Chandler wobble, a free oscillation with a period of 435 d (Smith & Dahlen 1981), or to diurnal body tides, which are impacted by resonant forcing associated with processes in the core and at the core-mantle boundary. The ultimate goal of our analysis is to provide a theoretical framework for using observations of the semi-diurnal and long-period body tide response—whether they are based on satellite-geodetic measurements or long-period seismic recordings—in a tomographic inversion procedure to constrain long-wavelength elastic, anelastic and/or density structure. Since the normal mode formalism we apply is semi-analytic, solving the forward problem is computationally inexpensive. This represents a significant advantage over numerical, finite-element approaches for predicting the body tide response (Métivier & Conrad 2008; Latychev *et al.* 2009).

We begin by briefly describing the harmonic representation of the luni-solar tidal forcing. We then describe our generalized normal mode treatment of the body tide response with emphasis on our adoption of advances in free oscillation seismology that post-date studies in the 1980s and our treatment of anelastic effects through the inclusion of relaxation modes. Next, we present some simple calculations for the case of a spherically symmetric, elastic and isotropic Earth model and compare these to results based on the traditional Love number theory (Farrell 1972); a comparison that highlights the link between the tidal problem and the long-period seismology problem. We then extend this test to calculate the frequency dependence of the Love numbers in the case of an anelastic Earth model. We also present body tide predictions for an Earth with aspherical mantle structure, and compare these with calculations based on a finite-volume simulation (Latychev *et al.* 2009). Finally, we explore the effects of rotation on the body tide response.

2 GENERAL THEORY

2.1 The tidal potential

The tidal potential for an observer whose origin is at the centre of mass of the Earth, $\Psi(\mathbf{r};t)$, can be expressed using the following harmonic representation (Cartwright & Edden 1973; Agnew 2007):

$$\Psi(\mathbf{r};t)=\sum_{\ell=2}^{\infty}\sum_{m=-\ell}^{\ell}\left(\frac{r}{a}\right)^{\ell}c_{\ell m}(t)Y_{\ell m}(\theta,\lambda), \tag{1}$$

where $Y_{\ell m}(\theta,\lambda)$ is the fully normalized spherical harmonic of degree ℓ and order m (Edmonds 1960), and t is time. The position vector $\mathbf{r}$ is specified by a radius $r=|\mathbf{r}|$, colatitude θ and longitude λ. The Earth's radius is denoted by a. The amplitude of the tidal potential decreases by a factor of $\approx 1/60$ with each increasing degree ℓ and so summation is often truncated at $\ell=4$ or lower. The coefficients $c_{\ell m}$ are represented as the sum of complex exponentials of various (real) frequencies and phases, as specified in tidal tables (Cartwright & Edden 1973):

$$c_{\ell m}(t)=\sum_{j}\mathcal{C}^{j}_{\ell m}\exp[i(\omega_j t+\eta_j)], \tag{2}$$

where $\mathcal{C}^j$, ω_j and η_j are the amplitude, frequency and phase of the jth harmonic, respectively. We can furthermore consider the tidal potential $\Psi(\mathbf{r};t)$ in the frequency domain, which we write as $\tilde{\Psi}(\mathbf{r};\omega)$ (and equivalently for $c_{\ell m}(t)$, $\tilde{c}_{\ell m}(\omega)$).

The most significant tides are the 'degree-2' tides, which naturally partition into three temporal bands: the semi-diurnal or sectorial band ($[\ell m]=[2,\pm 2]$), the diurnal or tesseral band ($[\ell m]=[2,\pm 1]$) and the long-period or zonal band ($[\ell m]=[2,0]$). The first descriptor in each case specifies the time dependence while the second refers to the spatial geometry of the forcing. The diurnal response is also impacted by resonant excitation due to the free-core nutation/nearly diurnal free wobble and involves additional rotational modes (Wahr & Bergen 1986). In the following discussion we avoid this complexity and focus on the semi-diurnal and long-period body tide response. In future work, we will extend the derivation to consider diurnal body tides.

2.2 Non-Hermitian operator

Over the last few decades, advances in seismology have yielded a perturbation theory that allows for the prediction of the long-period response on an aspherical, anelastic, rotating Earth due to earthquake sources (see Dahlen & Tromp 1998, for a review). Important contributions have been made by, for example, Dahlen (1968), Gilbert (1970), Woodhouse & Dahlen (1978), Woodhouse (1980), Park & Gilbert (1986) and Lognonné (1991); and more recently,

Deuss & Woodhouse (2001) and Deuss & Woodhouse (2004). The derivation outlined below makes full use of the present state of this theory, though we highlight the unique issues that arise in considering the response to a tidal potential forcing. The governing equation of motion in the frequency domain for a rotating, anelastic Earth due to a tidal forcing is

$$\mathcal{H}(\mathbf{r};\nu)\mathbf{s}(\mathbf{r}) - \nu^2\,\mathbf{s}(\mathbf{r}) + 2i\nu\,\boldsymbol{\Omega}\times\mathbf{s}(\mathbf{r}) = -\nabla\tilde{\Psi}(\mathbf{r};\nu), \quad \mathbf{r}\in V, \tag{3}$$

where V denotes the Earth's volume, $\mathbf{s}$ the displacement, ν the complex frequency, $\boldsymbol{\Omega}$ the angular rotation vector, and $i=\sqrt{-1}$. In practice, ν is dominated by the (real) forcing frequency, ω_T. The operator $\mathcal{H}$ is defined by

$$\begin{aligned}\rho(\mathbf{r})\,\mathcal{H}(\mathbf{r};\nu)\mathbf{s}(\mathbf{r}) = {}& \rho(\mathbf{r})\,\nabla\phi(\mathbf{r}) + \rho(\mathbf{r})\,\mathbf{s}(\mathbf{r})\cdot\nabla\nabla(\Phi(\mathbf{r})+\psi(\mathbf{r})) \\ & -\nabla\cdot[\boldsymbol{\Lambda}(\mathbf{r};\nu):\nabla\mathbf{s}(\mathbf{r})],\end{aligned} \tag{4}$$

where ρ is the mass density, and the equilibrium gravitational potential, centrifugal potential and incremental gravitational potential, Φ, ψ and ϕ, respectively, are given by

$$\Phi(\mathbf{r}) = -G\int_V \frac{\rho(\mathbf{r}')}{||\mathbf{r}-\mathbf{r}'||}\,\mathrm{d}V', \tag{5}$$

$$\psi(\mathbf{r}) = -\frac{1}{2}\left[\Omega^2 r^2 - (\boldsymbol{\Omega}\cdot\mathbf{r})^2\right], \tag{6}$$

$$\phi(\mathbf{r}) = -G\int_V \frac{\rho(\mathbf{r}')\,\mathbf{s}(\mathbf{r}')\cdot(\mathbf{r}-\mathbf{r}')}{||\mathbf{r}-\mathbf{r}'||^3}\,\mathrm{d}V'. \tag{7}$$

In these expressions, G is the universal gravitational constant and $\boldsymbol{\Lambda}$ is a fourth-order elastic tensor that defines the first Piola-Kirchhoff stress tensor. Eq. (3) is solved along with the following boundary condition:

$$\hat{\mathbf{n}}(\mathbf{r})\cdot[\boldsymbol{\Lambda}(\mathbf{r};\nu):\nabla\mathbf{s}(\mathbf{r})] = \mathbf{0},\ \mathbf{r}\in\partial V, \tag{8}$$

where ∂V is the surface of the Earth with unit outward normal $\hat{\mathbf{n}}$.

We note two important characteristics of this boundary value problem: the first is its nonlinearity in the eigenvalue parameter as a result of the frequency dependence of $\mathcal{H}$ and the second is its non-Hermitian nature (due to the complex parameterization of $\boldsymbol{\Lambda}$). These characteristics reflect the presence of dispersion and attenuation, both of which are a consequence of considering an anelastic Earth. $\boldsymbol{\Lambda}$ must satisfy the relation $\boldsymbol{\Lambda}^*(\nu)=\boldsymbol{\Lambda}(-\nu^*)$ (where the asterisk denotes complex conjugation) and must be analytic in the upper half of the complex ν plane to ensure reality and causality of the time domain response (Nowick & Berry 1972). Our treatment of $\boldsymbol{\Lambda}$ will be different from the commonly adopted approach in seismology, as will be discussed in Section 2.4.

Eqs (3) and (8) describe the forced motion of a conservative physical system, and in such systems the solution may be represented as a sum of the normal modes of the system (Gilbert 1970). Lognonné (1991) derived a theory to deal with the non-Hermitian nature of the boundary value problem in the seismic case. We apply his results next.

2.3 Duality and biorthogonality

Lognonné (1991) considered the eigenmodes of an Earth with the reversed sense of rotation, the so-called anti-Earth. In particular, he defined a dual space of adjoint eigenfunctions using a biorthogonality product. While this is the approach we will proceed with, other methodologies have been developed, for example, methods based on residue theory (Deuss & Woodhouse 2004). Following the notation in section 6.3 of Dahlen & Tromp 1998, if $\mathbf{s}_k$ are the eigenmodes for a rotating Earth and $\bar{\mathbf{s}}_k$ are the eigenmodes for an Earth rotating in the reversed sense, then there are two eigenvalue problems to be solved:

$$\mathcal{H}(\nu_k)\mathbf{s}_k + 2i\nu_k\boldsymbol{\Omega}\times\mathbf{s}_k - \nu_k^2\mathbf{s}_k = \mathbf{0}, \tag{9}$$

$$\mathcal{H}(\nu_k)\bar{\mathbf{s}}_k - 2i\nu_k\boldsymbol{\Omega}\times\bar{\mathbf{s}}_k - \nu_k^2\bar{\mathbf{s}}_k = \mathbf{0}. \tag{10}$$

Note, we have dropped the dependency on $\mathbf{r}$ from the relevant variables to avoid notational clutter. Lognonné (1991) showed that the eigenfrequency spectrum ν_k is the same regardless of the sense of rotation, though the eigenfunctions $\mathbf{s}_k$ and $\bar{\mathbf{s}}_k$ are different (with each mode k associated with a non-degenerate ν_k due to the presence of rotation). Let us define the duality product by

$$[\bar{\mathbf{s}}_k,\mathbf{s}_{k'}] = \int_V \rho\,\bar{\mathbf{s}}_k\cdot\mathbf{s}_{k'}\,\mathrm{d}V. \tag{11}$$

Using this duality product, the operator $\mathcal{H}$ is symmetric with respect to the following operations:

$$[\bar{\mathbf{s}}_k,\mathcal{H}(\nu_k)\mathbf{s}_{k'}] = [\mathcal{H}(\nu_k)\bar{\mathbf{s}}_k,\mathbf{s}_{k'}] = [\mathbf{s}_{k'},\mathcal{H}(\nu_k)\bar{\mathbf{s}}_k], \tag{12}$$

while the Coriolis operator is anti-symmetric:

$$[\bar{\mathbf{s}}_k, i\boldsymbol{\Omega}\times\mathbf{s}_{k'}] = -[i\boldsymbol{\Omega}\times\bar{\mathbf{s}}_k,\mathbf{s}_{k'}] = -[\mathbf{s}_{k'}, i\boldsymbol{\Omega}\times\bar{\mathbf{s}}_k]. \tag{13}$$

The anti-symmetry of the Coriolis operator is dealt with by introducing the anti-Earth, with rotation vector $-\boldsymbol{\Omega}$. Taking the duality product of $\mathcal{H}(\nu_k)\bar{\mathbf{s}}_k - 2i\nu_k\boldsymbol{\Omega}\times\bar{\mathbf{s}}_k = \nu_k^2\bar{\mathbf{s}}_k$ with $\mathbf{s}_{k'}$ yields

$$\nu_k^2[\mathbf{s}_{k'},\bar{\mathbf{s}}_k] + 2\nu_k[\mathbf{s}_{k'}, i\boldsymbol{\Omega}\times\bar{\mathbf{s}}_k] - [\mathbf{s}_{k'},\mathcal{H}(\nu_k)\bar{\mathbf{s}}_k] = 0, \tag{14}$$

and the duality product of $\mathcal{H}(\nu_{k'})\mathbf{s}_{k'} - 2i\nu_{k'}\boldsymbol{\Omega}\times\mathbf{s}_{k'} = \nu_{k'}^2\mathbf{s}_{k'}$ with $\bar{\mathbf{s}}_k$ gives

$$\nu_{k'}^2[\bar{\mathbf{s}}_k,\mathbf{s}_{k'}] - 2\nu_{k'}[\bar{\mathbf{s}}_k, i\boldsymbol{\Omega}\times\mathbf{s}_{k'}] - [\bar{\mathbf{s}}_k,\mathcal{H}(\nu_{k'})\mathbf{s}_{k'}] = 0. \tag{15}$$

Subtracting eq. (15) from eq. (14) and dividing by $(\nu_k^2-\nu_{k'}^2)$ provides the following biorthogonal relation between eigenmodes $\mathbf{s}_{k'}$ and $\bar{\mathbf{s}}_k$:

$$[\bar{\mathbf{s}}_k,\mathbf{s}_{k'}] - \frac{2}{\nu_k+\nu_{k'}}[\bar{\mathbf{s}}_k, i\boldsymbol{\Omega}\times\mathbf{s}_{k'}] - \frac{[\bar{\mathbf{s}}_k,\{\mathcal{H}(\nu_k)-\mathcal{H}(\nu_{k'})\}\mathbf{s}_{k'}]}{\nu_k^2-\nu_{k'}^2} = 0, \tag{16}$$

where $\nu_k\neq\nu_k$, along with the following normalization for the case $\nu_{k'}=\nu_k$:

$$[\bar{\mathbf{s}}_k,\mathbf{s}_k] - \frac{1}{\nu_k}[\bar{\mathbf{s}}_k, i\boldsymbol{\Omega}\times\mathbf{s}_k] - \frac{1}{2\nu_k}[\bar{\mathbf{s}}_k,\partial_\nu\mathcal{H}(\nu_k)\mathbf{s}_k] = 1. \tag{17}$$

2.4 Anelasticity over the tidal timescale

Anelasticity causes both dispersion and attenuation of the response, and manifests itself differently in body tides and the response to earthquakes. In particular, attenuation gives rise to decaying sinusoids for the earthquake response and to a phase lag in the tidal response. Wahr & Bergen (1986) were the first to perform theoretical studies of the body tide on an anelastic Earth and concluded that anelastic effects perturbed the response at the per cent level relative to the elastic case. Their approach, however, did not describe precisely how attenuation affects each mode. As we demonstrate in this section, such a description is possible within the theoretical framework outlined in Sections 2.2 and 2.3. Nevertheless, in deriving our approach we will highlight significant differences in our treatment of anelasticity for the tidal application relative to the approach commonly adopted in the seismic free oscillation literature.

The effect of anelasticity is captured within the term $\mathbf{\Lambda}(\nu)$, where for an isotropic medium

$$\Lambda_{ijkl}(\nu) = \left[\kappa(\nu) - \frac{2}{3}\mu(\nu)\right]\delta_{ij}\delta_{kl} + \mu(\nu)[\delta_{ik}\delta_{jl} + \delta_{il}\delta_{jk}] + \frac{1}{2}\big(T^0_{ij}\delta_{kl} + T^0_{kl}\delta_{ij} + T^0_{ik}\delta_{jl} - T^0_{jk}\delta_{il} - T^0_{il}\delta_{jk} - T^0_{jl}\delta_{jk} - T^0_{jl}\delta_{ik}\big). \quad (18)$$

Here, μ is the shear modulus, κ is the bulk modulus and δ_{ij} is the Kronecker delta. $\mathbf{T}^0$ is the initial stress tensor. The moduli μ and κ are in general spatially variable, though to avoid clutter we do not explicitly write this dependence. Three aspects related to the form of $\mathbf{\Lambda}(\nu)$ must be considered in solving for the tidal response. These are: (i) anelastic eigenfrequencies, (ii) anelastic eigenfunctions, and (iii) the presence of normal modes beyond the usual set considered in seismic applications. Across seismic timescales, $\mathbf{\Lambda}(\nu)$ is commonly built through a superposition of standard linear solids (or Zener solids; Liu *et al.* 1976). The superposition is often dictated by measurements of Q_k, the quality-factor of a mode k, across the seismic frequency range. This parameter is related to, but not to be confused with, the intrinsic Q of an anelastic solid, defined formally by O'Connell & Budiansky (1978) as

$$Q_M(\omega) = \frac{\mathrm{Re}\{M(\omega)\}}{\mathrm{Im}\{M(\omega)\}}, \quad (19)$$

where M may be substituted for μ or κ, and ω is a real frequency. Examples of $\mathbf{\Lambda}(\nu)$ include the constant-Q absorption band model (Kanamori & Anderson 1977), which is most widely used in seismology, and the frequency-dependent Q model (Anderson & Minster 1979). It has been shown, both experimentally (e.g. Jackson *et al.* 2002) and observationally (e.g. Benjamin *et al.* 2006; Lekić *et al.* 2009), that Q is frequency dependent within and beyond the seismic band, and this is commonly described by a power-law dependency with frequency.

Expressions for the anelastic eigenfrequencies may be derived via a complex, first-order perturbation to the elastic eigenfrequency, ω^e_k, such that

$$\nu_k = \omega^e_k + \delta\omega_k + i\gamma_k, \quad (20)$$

where $\delta\omega_k$ and γ_k are real, and we define $\omega_k \equiv \mathrm{Re}\{\nu_k\} = \omega^e_k + \delta\omega_k$. The dispersive perturbation, $\delta\omega_k$, is found by considering the real part of $\mu(\nu)$ and $\kappa(\nu)$ perturbed from some reference value:

$$\mu(\nu) \to \mu_R + \delta\mu(\nu), \quad (21)$$

$$\kappa(\nu) \to \kappa_R + \delta\kappa(\nu). \quad (22)$$

The attenuative perturbation, γ_k (the inverse decay time of a mode), is related to Q_k^{-1} by

$$Q_k^{-1} = \frac{2\gamma_k}{\omega_k} \quad (23)$$

and is dependent upon how that particular mode samples the Q_μ and Q_κ structure of the Earth. Q_k may be determined by taking the imaginary component of eq. (14) with eigenfunctions $\mathbf{s}_k$ and $\mathbf{s}^*_k$, along with the symmetry relation $\mathbf{\Lambda}_{ijkl} = \mathbf{\Lambda}_{klij}$, to yield the relation

$$2\,\mathrm{Re}\{\nu_k\}\mathrm{Im}\{\nu_k\}\left(\int_V \rho\,\mathbf{s}^*_k\cdot\mathbf{s}_k\,\mathrm{d}V - \omega_k^{-1}\int_V \rho\,\mathbf{s}^*_k\cdot(i\mathbf{\Omega}\times\mathbf{s}_k)\mathrm{d}V\right) = \int_V \nabla\mathbf{s}^*_k : \mathrm{Im}\{\mathbf{\Lambda}(\nu_k)\} : \nabla\mathbf{s}_k\,\mathrm{d}V; \quad (24)$$

and using eq. (23) one finds

$$Q_k^{-1} = \frac{\int_V \kappa(\omega_k)Q_\kappa^{-1}(\omega_k)(\nabla\cdot\mathbf{s}^*_k)(\nabla\cdot\mathbf{s}_k) + 2\mu(\omega_k)Q_\mu^{-1}(\omega_k)(\mathbf{d}^*_k : \mathbf{d}_k)\,\mathrm{d}V}{\omega_k^2\left[\int_V \rho\,\mathbf{s}^*_k\cdot\mathbf{s}_k\,\mathrm{d}V - \omega_k^{-1}\int_V \rho\,\mathbf{s}^*_k\cdot(i\mathbf{\Omega}\times\mathbf{s}_k)\mathrm{d}V\right]}. \quad (25)$$

Here, we have made no assumption about the form that the superposition of standard linear solids may take. Furthermore, Q_μ and Q_κ may or may not be frequency dependent. Over tidal timescales it is reasonable to expect that Q would be frequency dependent.

In seismic applications for spherically symmetric Earth models, the treatment of anelasticity would end with the expressions above for anelastic eigenfrequencies. However, anelastic Earth models will also be characterized by complex eigenfunctions. These may be similarly determined by a complex perturbation to the elastic eigenfunctions, thereby introducing a phase shift. The impact of complex eigenfunctions is thought to be negligible in the seismic normal mode problem (Tromp & Dahlen 1990). However, since lower frequency processes are affected to a greater extent by anelasticity, this may not be the case in the tidal application.

Tromp & Dahlen (1990) derived a free oscillation treatment that accounts for exact anelasticity on a non-rotating Earth by coupling the modes of an elastic, non-rotating Earth, $\mathbf{s}^e_k$, with associated eigenfrequencies, ω^e_k. We follow a similar procedure, though we will extend their approach to incorporate rotation. Let us expand the anelastic modes of the Earth, $\mathbf{s}_k$, as follows

$$\mathbf{s}_k = \sum_{k'} \chi_{kk'}\mathbf{s}^e_{k'}, \quad (26)$$

where $\chi_{kk'}$ is complex. Using this expression in eq. (9) and taking the inner product with $\mathbf{s}^{e*}_k$ leaves

$$[\boldsymbol{\omega}^2 + \mathbf{V}(\nu) + 2\nu\mathbf{W} - \boldsymbol{\nu}^2]\boldsymbol{\chi} = \mathbf{0}, \quad (27)$$

where $\boldsymbol{\omega}^2 = \mathrm{diag}\,\{[\omega^e_k]^2\}$ and $\boldsymbol{\nu}^2 = \mathrm{diag}\,\{\nu_k^2\}$. Modes on a non-rotating and elastic Earth are normalized according to

$$\int_V \rho\,\mathbf{s}^{e*}_k\cdot\mathbf{s}^e_{k'}\,\mathrm{d}V = \delta_{kk'}. \quad (28)$$

Eq. (27) arises as we decompose $\mathcal{H}$ into its unperturbed (elastic) and perturbed parts: that is, $[\mathbf{s}^e_k, \mathcal{H}^e\mathbf{s}_k] = [\omega^e_k]^2$ and we define $V_{kk'}(\nu) \equiv [\mathbf{s}^{e*}_k, \delta\mathcal{H}(\nu)\mathbf{s}^e_{k'}]$, whose matrix elements are

$$V_{kk'}(\nu) = \int_V \delta\kappa(\nu)(\nabla\cdot\mathbf{s}^{e*}_k)(\nabla\cdot\mathbf{s}^e_{k'})\,\mathrm{d}V + 2\int_V \delta\mu(\nu)\,\mathbf{d}^{e*}_k : \mathbf{d}^e_{k'}\,\mathrm{d}V \quad (29)$$

and elements of the matrix $\mathbf{W}$ are given by

$$W_{kk'} = \int_V \rho\,\mathbf{s}^{e*}_k\cdot(i\mathbf{\Omega}\times\mathbf{s}^e_{k'})\mathrm{d}V. \quad (30)$$

As in Section 2.3, we must also consider the system of the anti-Earth where anelastic modes are denoted as

$$\bar{\mathbf{s}}_k = \sum_{k'} \overline{\chi}_{kk'}\mathbf{s}^{e*}_{k'}, \quad (31)$$

where the coefficients $\overline{\boldsymbol{\chi}}$ are prescribed by the equation

$$[\boldsymbol{\omega}^2 + \mathbf{V}(\nu) - 2\nu\mathbf{W} - \boldsymbol{\nu}^2]\overline{\boldsymbol{\chi}} = \mathbf{0}. \quad (32)$$

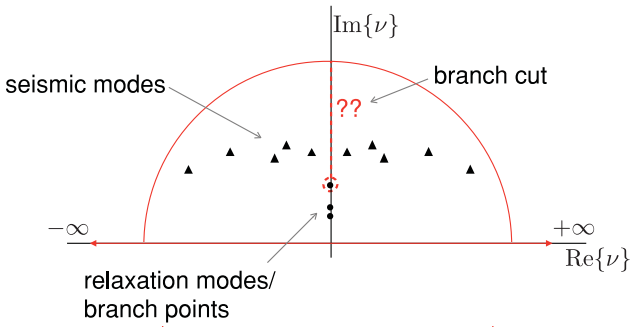

Figure 1. A schematic illustration of the location of eigenfrequencies relevant to the tidal problem on the complex plane. The red line indicates how the Bromwich contour may be deformed in applying Cauchy residue theory to determine the time domain response.

The normalization of the eigenvectors, $\boldsymbol{\chi}$ and $\overline{\boldsymbol{\chi}}$, is defined by

$$\sum_{k'} \overline{\chi}_{kk'}\,\chi_{k'k} - \frac{1}{\nu_k}\sum_{k',k''} \overline{\chi}_{k''k} W_{k''k'}\chi_{k'k} - \frac{1}{2\,\nu_k}\sum_{k',k''} \overline{\chi}_{k''k}\,\partial_\nu V_{k''k'}(\nu_k)\chi_{k'k} = 1. \tag{33}$$

The matrix $\mathbf{V}$ governs how modes couple through anelasticity and performing the diagonalization of eq. (27) provides the expansion coefficients necessary in eq. (26) and similarly eqs (31) and (32). Thus far we have made no assumption about the aspherical structure of this Earth model. Aspherical structure and rotation cause coupling across modes of different degrees, together with coupling of non-degenerate orders of $2\ell + 1$ within each mode, as a result of the broken symmetry. In Section 2.5 we discuss this coupling. If we assume a non-rotating Earth with spherically symmetric anelastic structure, only coupling between $(2\ell + 1)$-degenerate modes of same degree but different overtones occurs. It is unlikely that current uncertainties in geodetic measurements of body tides allow for constraints to be placed on aspherical dissipation (e.g. Kim & Shibuya 2013).

The final issue to be addressed concerns an additional set of normal modes that become important at lower frequencies beyond the seismic band. Within the seismic band, anelastic eigenfrequencies are found in the complex plane just above the real frequency axis. As we have discussed, the set of ω_k are found using perturbation theory and their associated departure from the real axis, $i\gamma_k$, is determined by considering the Q structure at their real frequencies, ω_k. However, a set of modes also exists along the imaginary axis (Yuen & Peltier 1982). These relaxation modes (referred to as 'quasi-static modes' in Yuen & Peltier 1982) are purely decaying modes and they are analogous to normal modes treated in studies of glacial isostatic adjustment (e.g. Wu 1978; Tromp & Mitrovica 1999).

Fig. 1 is a schematic diagram illustrating the location of this complete set of modes on the complex plane. Al-Attar (2007) demonstrated that summation of the signal associated with this set of modes to form a time-domain response (see Section 2.6) is equivalent to inverting the frequency-domain response by Cauchy's residue theorem (see also Wu 1978). For such an inversion, the Bromwich line that runs along the real axis from $[-\infty, +\infty]$ is deformed to form a semicircle over the upper half of the complex plane in the case of $t > 0$. Singularities found along the imaginary axis may be modal (i.e. poles) or, more likely for the Earth, multi-valued, in which case the Bromwich line must be further deformed to consider branch cuts. To avoid confusion, we will use the term 'seismic modes' when discussing modes near the real axis, and 'relaxation modes' for those along the imaginary axis. In Section 3.1.2, we use a simple example to demonstrate that the inclusion of the relaxation modes is necessary for the accurate incorporation of anelastic effects within our normal mode formalism for computing the tidal response.

2.5 Perturbation theory for an aspherical Earth

In this section we specify how to use the framework described above to consider an Earth with aspherical mantle structure. We note that Qin *et al.* (2014) have recently derived a semi-analytical perturbation theory to predict the impact of aspherical elastic structure on lunar body tides. In contrast to the normal mode approach described herein, their perturbation theory is applied directly to the differential equations of motion and perturbed gravity. Moreover, the Qin *et al.* (2014) approach treats the underlying coupling between modes of deformation in stages, whereas our normal mode approach treats the full coupling in one step, and their study does not include the consideration of rotational effects, which is a significantly smaller effect on tidal deformation of the Moon.

Following Dahlen & Tromp (1998), we restate the deformation problem in the form of a variational principle (Rayleigh's principle) where the action, $\mathcal{I}$, is defined as

$$\mathcal{I} = \frac{1}{2}\nu^2[\overline{\mathbf{s}}, \mathbf{s}] - \nu[\overline{\mathbf{s}}, i\boldsymbol{\Omega}\times\mathbf{s}] - \frac{1}{2}[\overline{\mathbf{s}}, \mathcal{H}(\nu)\mathbf{s}]. \tag{34}$$

Note that eq. (34) holds for both a spherically symmetric and aspherical Earth. To first order, the variation in this expression is given by

$$\delta\mathcal{I} = \frac{1}{2}[\delta\overline{\mathbf{s}}, \nu^2\mathbf{s} - 2i\nu\boldsymbol{\Omega}\times\mathbf{s} - \mathcal{H}(\nu)\mathbf{s}] + \frac{1}{2}[\delta\mathbf{s}, \nu^2\overline{\mathbf{s}} + 2i\nu\boldsymbol{\Omega}\times\overline{\mathbf{s}} - \mathcal{H}(\nu)\overline{\mathbf{s}}], \tag{35}$$

where we have made use of the duality product (eqs 11–13). If, and only if, $\mathbf{s}$ and $\overline{\mathbf{s}}$ are the eigenfunctions for the Earth and anti-Earth, respectively, and have the associated eigenfrequencies ν_k, then $\delta\mathcal{I} \to 0$ for arbitrary and independent variations of $\delta\overline{\mathbf{s}}$ and $\delta\mathbf{s}$.

We next introduce an Earth model with small lateral variations in structure:

$$\rho(\mathbf{r}) = \rho^0(r) + \delta\rho(\mathbf{r}), \tag{36}$$

$$\mu(\mathbf{r}) = \mu^0(r) + \delta\mu(\mathbf{r}), \tag{37}$$

$$\kappa(\mathbf{r}) = \kappa^0(r) + \delta\kappa(\mathbf{r}), \tag{38}$$

where hereafter the superscript '0' denotes spherically symmetric quantities. We note that the introduction of aspherical structure implies the existence of deviatoric pre-stress. Woodhouse & Dahlen (1978) derived a general form of the seismic normal mode problem that included deviatoric pre-stresses. However, Dahlen (1972) investigated the contribution of this stress field on the wave propagation problem and found that it could be neglected since the ratio of non-hydrostatic stresses over the isotropic stress is small. The ratio is also small for the tidal problem, and so in the following derivation we neglect any deviatoric pre-stress.

To continue, we expand the eigenfunctions of the aspherical Earth and anti-Earth, $\mathbf{s}$ and $\overline{\mathbf{s}}$, using the unperturbed, $(2\ell + 1)$-degenerate, singlet basis functions $\mathbf{s}_k^0$ as follows

$$\mathbf{s} = \sum_k q_k \mathbf{s}_k^0, \tag{39}$$

$$\overline{\mathbf{s}} = \sum_k \overline{q}_k \mathbf{s}_k^{0*}, \tag{40}$$

where the expansion depends on weights $\overline{q}_k$ and q_k. These unperturbed eigenfunctions are those associated with a spherical, non-rotating, elastic and isotropic (SNREI) Earth. Substituting these expansions into the action $\mathcal{I}$ (eq. 34) yields

$$\mathcal{I} = \frac{1}{2}\overline{\mathbf{q}}^T[\nu^2\mathbf{T} - 2\nu\mathbf{W} - \mathbf{V}'(\nu)]\mathbf{q}, \tag{41}$$

where elements of the kinetic energy matrix $\mathbf{T}$, the potential energy matrix $\mathbf{V}'$ and the Coriolis matrix $\mathbf{W}$ are given by

$$T_{kk'} = \int_V \rho\, \mathbf{s}_k^{0*} \cdot \mathbf{s}_{k'}^0 \mathrm{d}V, \tag{42}$$

$$V'_{kk'} = \int_V \rho\, \mathbf{s}_k^{0*} \cdot \mathcal{H}(\nu)\mathbf{s}_{k'}^0 \mathrm{d}V \tag{43}$$

$$W_{kk'} = \int_V \rho\, \mathbf{s}_k^{0*} \cdot i\boldsymbol{\Omega} \times \mathbf{s}_{k'}^0 \mathrm{d}V. \tag{44}$$

We label the matrix $\mathbf{V}'$ to avoid confusion with the matrix $\mathbf{V}$ in Section 2.4, though they both act to perturb the potential energy. The variation of eq. (41) (i.e. eq. 35) may be written as

$$\delta\mathcal{I} = \frac{1}{2}\delta\overline{\mathbf{q}}^T[\nu^2\mathbf{T} - 2\nu\mathbf{W} - \mathbf{V}'(\nu)]\mathbf{q} + \frac{1}{2}\delta\mathbf{q}^T[\nu^2\mathbf{T} + 2\nu\mathbf{W} - \mathbf{V}'(\nu)]\overline{\mathbf{q}}, \tag{45}$$

where $\mathbf{T}^T = \mathbf{T}$, $\mathbf{V}'^T(\nu) = \mathbf{V}'(\nu)$ and $\mathbf{W}^T = -\mathbf{W}$. If, and only if, $\mathbf{q}$ and $\overline{\mathbf{q}}$ are the eigenvector and dual eigenvector with associated eigenfrequency ν, then for arbitrary and independent variations $\delta\mathbf{q}$ and $\delta\overline{\mathbf{q}}$, the variation $\delta\mathcal{I} \to 0$, leaving two quadratic eigenvalue problems:

$$[\mathbf{V}'(\nu) + 2\nu\mathbf{W} - \nu^2\mathbf{T}]\mathbf{q} = \mathbf{0} \tag{46}$$

$$[\mathbf{V}'(\nu) - 2\nu\mathbf{W} - \nu^2\mathbf{T}]\overline{\mathbf{q}} = \mathbf{0}. \tag{47}$$

To implement these perturbations in Earth structure, we express the density and elastic structure in terms of spherical harmonics:

$$\rho(r,\theta,\lambda) = \sum_{s=1}^{s_{\max}} \sum_{t=-s}^{t=s} \delta\rho_{st}(r) Y_{st}(\theta,\lambda), \tag{48}$$

$$\kappa(r,\theta,\lambda) = \sum_{s=1}^{s_{\max}} \sum_{t=-s}^{t=s} \delta\kappa_{st}(r) Y_{st}(\theta,\lambda), \tag{49}$$

$$\mu(r,\theta,\lambda) = \sum_{s=1}^{s_{\max}} \sum_{t=-s}^{t=s} \delta\mu_{st}(r) Y_{st}(\theta,\lambda), \tag{50}$$

where s and t are harmonic degree and order, respectively. The manner in which a pair of singlet (or reference) eigenmodes $\mathbf{s}_k$ and $\mathbf{s}_{k'}$ interact in the presence of structure $\{s,t\}$ is determined by order-independent Woodhouse kernels (Woodhouse 1980), which were extended by Mochizuki (1986) to include the effects of transverse anisotropy. To illustrate how these kernels are used to populate the relevant matrices, consider the following simplified expressions:

$$T_{kk'} = \delta_{kk'} + \sum_{st} \zeta(\ell,m;\ell',m';s,t) \int_0^a \delta\rho_{st} T_\rho^{\ell s\ell'} r^2 \mathrm{d}r; \tag{51}$$

$$V_{kk'} = [\nu_k^0]^2\delta_{kk'} + \sum_{st} \zeta(\ell,m;\ell',m';s,t) \times \int_0^a \left(\delta\kappa_{st} V_\kappa^{\ell s\ell'} + \delta\mu_{st} V_\mu^{\ell s\ell'} + \delta\rho_{st} V_\rho^{\ell s\ell'}\right) r^2 \mathrm{d}r. \tag{52}$$

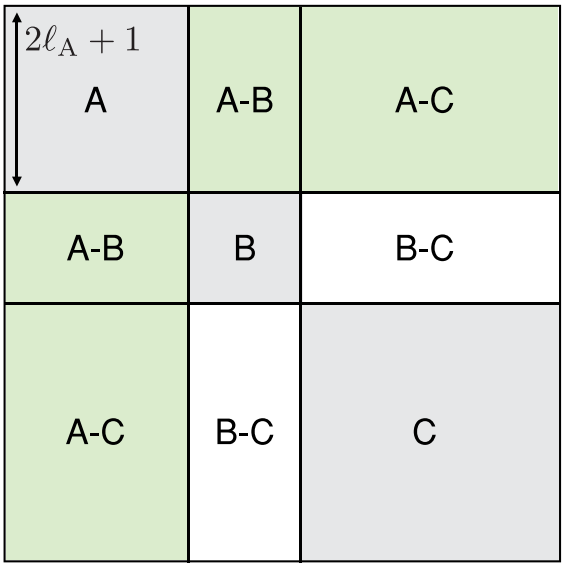

Figure 2. A schematic illustration of either matrix $\mathbf{T}$ or $\mathbf{V}'$ for the simple case of only three normal modes: A, B and C. The square, on-diagonal submatrices are self-coupling matrices. The dimensions of each self-coupling matrix is $(2\ell+1)\times(2\ell+1)$, and ℓ_A is the degree of mode A. The off-diagonal submatrices are cross-coupling matrices. If mode A is of the same degree and order as the forcing, the coupling of modes with A is termed 'direct coupling' (shown by green-shaded submatrices). All other cross-couplings are termed 'indirect couplings' (shown by unshaded submatrices).

Here, ζ represents a pre-factor that dictates the modal interactions expressed via Wigner 3-j symbols. Note that we have replaced the index k used in previous sections to make explicit the dependence of each mode on spherical harmonic degree and order, ℓ and m, respectively, and the overtone number, n. ζ gives rise to what is commonly known as a 'selection rule' between modes and a given structure. Selection rules (i.e. whether two modes will couple) are governed by the geometry of the modes and the structure in question. $T_\rho^{\ell s\ell'}$, $V_\kappa^{\ell s\ell'}$, $V_\mu^{\ell s\ell'}$ and $V_\rho^{\ell s\ell'}$ are the Woodhouse kernels which are formed by combining the reference eigenfunctions of modes k and k'. Additional kernels also exist for aspherical discontinuities. For the case of N modes, this results in a matrix of N^2 submatrices. Explicit expressions for the matrix elements may be found in Woodhouse 1980. [Note that the expressions in this paper assume real spherical harmonics, whereas those in Woodhouse (1980) assume complex spherical harmonics. The appropriate transformation from real to complex spherical harmonics can be found in appendix D of Dahlen & Tromp (1998).]

Fig. 2 provides a schematic representation of either matrix $\mathbf{T}$ or $\mathbf{V}'$ in the case when only three modes, A, B and C, are considered. (In practice, many more modes are considered.) The square, on-diagonal submatrices (shaded grey), labelled 'A', 'B' and 'C', are submatrices associated with self-coupling within each mode. These submatrices are $(2\ell+1)\times(2\ell+1)$ in size, where ℓ is the degree of the mode in question. The off-diagonal matrices are cross-coupling matrices; that is, they govern interactions between different modes. After diagonalizing this matrix, the interactions of all the modes form the new eigenfunctions $\mathbf{s}$ (and $\overline{\mathbf{s}}$) in one step. In Section 3.2, we revisit this schematic illustration when considering how the selection rules play a role in the tidal response of an aspherical Earth.

2.6 Semi-diurnal or long-period body tide response

Eqs (9), (10), (16) and (17) provide a framework for predicting the semi-diurnal or long-period response of an aspherical, rotating and anelastic Earth to tidal forcing. Using these relations, the eigenmodes combine to form the rotating, anelastic Earth's Green's function, **G**, given by (Lognonné 1991):

$$\mathbf{G}(\mathbf{r},\mathbf{r}';t)=\sum_k (2i\nu_k)^{-1}\mathbf{s}_k(\mathbf{r})\bar{\mathbf{s}}_k(\mathbf{r}')\exp(i\nu_k t). \tag{53}$$

When considering only the seismic modes, one notes that if ν_k and $\mathbf{s}_k$ are eigenfrequencies and eigenfunctions of the Earth, then, according to the relation stated in Section 2.2 (where $\mathbf{\Lambda}^*(\nu)=\mathbf{\Lambda}(-\nu^*)$ to satisfy causality in the time domain), so too are $-\nu_k^*$ and $\mathbf{s}_k^*$. It follows that in seismological applications, where relaxation modes are ignored, the Green's function may be stated as

$$\mathbf{G}(\mathbf{r},\mathbf{r}';t)=\mathrm{Re}\sum_k (i\nu_k)^{-1}\mathbf{s}_k(\mathbf{r})\bar{\mathbf{s}}_k(\mathbf{r}')\exp(i\nu_k t), \tag{54}$$

including only modes where $\mathrm{Re}\{\nu_k\}>0$ in the summation. However, by using eq. (53) the displacement tidal response, **s**, is then computed via a space-time convolution:

$$\begin{aligned}\mathbf{s}(\mathbf{r},t)=&-\int_{-\infty}^{t}\int_{V'}\rho(\mathbf{r}')\,\mathbf{G}(\mathbf{r},\mathbf{r}';t-t')\cdot\nabla\Psi(\mathbf{r}',t')\,\mathrm{d}V'\mathrm{d}t'\\&-\int_{-\infty}^{t}\int_{V'}\rho(\mathbf{r}')\,\mathbf{B}(\mathbf{r},\mathbf{r}';t-t')\cdot\nabla\Psi(\mathbf{r}',t')\,\mathrm{d}V'\mathrm{d}t'.\end{aligned} \tag{55}$$

The term **B** is the contribution from any branch cuts. In general, the time integration of the Green's function will yield a transient response upon initiation of the forcing. If we begin the forcing well before the observation time t, this transient response will be unimportant. Accordingly, we begin the time integration at $t'=-\infty$ to isolate the steady-state solution.

The eigenmodes $\mathbf{s}_k$ and $\bar{\mathbf{s}}_k$ have two forms: spheroidal and toroidal (commonly labelled as ${}_n\mathcal{S}_{\ell m}$ and ${}_n\mathcal{T}_{\ell m}$, respectively). These can be highlighted by decomposing **s** into contributions from each eigenfunction $\mathcal{U}_k$, $\mathcal{V}_k$ and $\mathcal{W}_k$:

$$\mathbf{s}=\sum_{n,\ell,m}{}_n\mathcal{U}_{\ell m}\mathbf{P}_{\ell m}+{}_n\mathcal{V}_{\ell m}\mathbf{B}_{\ell m}+{}_n\mathcal{W}_{\ell m}\mathbf{C}_{\ell m}, \tag{56}$$

$$\mathbf{s}=\sum_{n,\ell,m}{}_n\overline{\mathcal{U}}_{\ell m}\mathbf{P}_{\ell m}+{}_n\overline{\mathcal{V}}_{\ell m}\mathbf{B}_{\ell m}+{}_n\overline{\mathcal{W}}_{\ell m}\mathbf{C}_{\ell m}. \tag{57}$$

The terms involving $\mathcal{U}_k$ and $\mathcal{V}_k$ constitute the spheroidal modes and the last term with $\mathcal{W}_k$ constitutes the toroidal modes. $\mathbf{P}_{\ell m}$, $\mathbf{B}_{\ell m}$ and $\mathbf{C}_{\ell m}$ are the vector spherical harmonics

$$\mathbf{P}_{\ell m}=Y_{\ell m}\hat{\mathbf{r}}, \tag{58}$$

$$\mathbf{B}_{\ell m}=\frac{1}{\sqrt{\ell(\ell+1)}}\nabla_1 Y_{\ell m}, \tag{59}$$

$$\mathbf{C}_{\ell m}=-\frac{1}{\sqrt{\ell(\ell+1)}}\hat{\mathbf{r}}\times\nabla_1 Y_{\ell m}, \tag{60}$$

and ${}_n\mathcal{U}_{\ell m}$ (or $\mathcal{U}_k$), ${}_n\mathcal{V}_{\ell m}$ (or $\mathcal{V}_k$) and ${}_n\mathcal{W}_{\ell m}$ (or $\mathcal{W}_k$) are the complex displacement eigenfunctions found by substituting eq. (56) into eq. (26), which yields

$$\mathcal{U}_k=\sum_{k'}\chi_{kk'}U_{k'}, \tag{61}$$

$$\mathcal{V}_k=\sum_{k'}\chi_{kk'}V_{k'}, \tag{62}$$

$$\mathcal{W}_k=\sum_{k'}\chi_{kk'}W_{k'}, \tag{63}$$

where U_k, V_k and W_k are the real unperturbed eigenfunctions. We emphasize this distinction to highlight the effects discussed in Section 2.4. For spherically symmetric seismic applications, $\boldsymbol{\chi}$ would simply be approximated as the identity matrix. In any event, convolving the Green's function, **G**, which involves the summation of modes defined by relations in Section 2.3, with the time-domain forcing, yields the tidal response.

3 SOME ILLUSTRATIVE CASE STUDIES

The calculations below have two purposes: first, to illustrate predictions based on the normal mode theory we have developed, and, second, to compare these predictions with either published results or results generated using an independent, finite-volume numerical scheme. These case studies are divided into two parts: Section 3.1 considers only spherically symmetric Earth models and Section 3.2 uses the perturbation theory described in Section 2.5 to consider aspherical Earth models. We note that the eigenfunctions and eigenfrequencies within the seismic band for any given spherically symmetric Earth model were computed using the software MINEOS (Woodhouse 1988; Masters *et al.* 2007).

3.1 Spherical Earth

3.1.1 Elastic Earth

In this subsection, we treat the simplest case of an SNREI Earth model. We introduce the basis functions for this Earth model, which in turn form the basis functions for the response of an anelastic Earth (see Section 2.4). In the SNREI case, two simplifications are made: $\mathbf{\Lambda}$ is purely real and $\boldsymbol{\Omega}=\mathbf{0}$. Thus, only one of the two eigenvalue problems (eqs 9 and 10) needs to be solved since the Coriolis operator vanishes.

For the present, elastic Earth model case, the Green's function approach outlined in Section 2.6 requires a minor modification. In particular, since there is no dissipation in the system, the extra transient terms that appear at the onset of forcing do not disappear, in contrast to their decay in the anelastic case. So, in this subsection we solve the time-harmonic problem (with no initial conditions) given by the non-rotating, elastic version of eq. (3):

$$\mathcal{H}^e\mathbf{s}-[\omega_T]^2\mathbf{s}=-\nabla\tilde{\Psi}(\mathbf{r};\omega_T), \tag{64}$$

where we expand the solution, **s** as

$$\mathbf{s}=\sum_k\beta_k\mathbf{s}_k. \tag{65}$$

The β_k are coefficients to be determined. Substituting this expansion into eq. (64) and using the relation

$$[\omega_k]^2\mathbf{s}_k=\mathcal{H}^e\mathbf{s}_k, \tag{66}$$

which is satisfied if $\mathbf{s}_k$ is an eigenfunction of $\mathcal{H}^e$, yields

$$\left([\omega_k^e]^2-\omega_T^2\right)\sum_k\beta_k\mathbf{s}_k=-\nabla\tilde{\Psi}. \tag{67}$$

Taking the inner product of eq. (67) with $\mathbf{s}_k^*$ yields an expression for β_k:

$$\beta_k = \frac{1}{\omega_k^2 - \omega_T^2} \frac{[-\nabla\tilde{\Psi}, \mathbf{s}_k^*]}{[\mathbf{s}_k, \mathbf{s}_k^*]}. \tag{68}$$

Note that the normalization for an SNREI Earth model is $[\mathbf{s}_k, \mathbf{s}_{k'}^*] = 1$ when $k = k'$ and 0 otherwise. Using this normalization yields the time-domain response:

$$\mathbf{s}(\mathbf{r}; t) = -\sum_k \frac{\mathbf{s}_k(\mathbf{r})}{\omega_k^2 - \omega_T^2} \int_{V'} \rho(\mathbf{r}')\mathbf{s}_k^*(\mathbf{r}') \cdot \nabla\tilde{\Psi}(\mathbf{r}; \omega_T) \exp[i\omega_T t] \mathrm{d}V'. \tag{69}$$

Finally, using eq. (1), we have

$$\nabla\tilde{\Psi}(\mathbf{r}; \omega_T) = -\sum_{\ell=0}^{\infty} \sum_{m=-\ell}^{m=\ell} \tilde{c}_{\ell m}(\omega_T) \times \frac{r^{\ell-1}}{a^\ell} \left[\ell \mathbf{P}_{\ell m}(\theta, \lambda) + \sqrt{\ell(\ell+1)}\mathbf{B}_{\ell m}(\theta, \lambda)\right]. \tag{70}$$

We will compare results generated using eqs (69)–(70) with Love numbers for an SNREI Earth computed using the formalism outlined by Farrell (1972). The radial- and degree-dependent dimensionless Love numbers are defined by the expressions

$$s_r(\mathbf{r}; t) = \sum_\ell \frac{h_\ell(r)}{g} \Psi(\mathbf{r}; t), \tag{71}$$

$$\mathbf{s}_t(\mathbf{r}; t) = \sum_\ell \frac{l_\ell(r)}{g} \nabla\Psi(\mathbf{r}; t). \tag{72}$$

Here, s_r and $\mathbf{s}_t$ are the radial and tangential displacement, respectively, and h and l are the Love numbers associated with these displacements. The Love number calculation ignores inertia and computing these numbers involves solving a coupled system of first-order differential equations that are expressed in a general propagator form (Farrell 1972). In the normal mode formalism, the static Love numbers are given by the following expressions once eq. (69) is calculated and assuming no inertia (i.e. $\omega_T \to 0$).

$$h_\ell(r) = -g \sum_{n=0}^{\infty} \frac{{}_nU_\ell(r)}{{}_n\omega_\ell^2} \times \int_0^a \rho \frac{r^{\ell+1}}{a_\ell} \left[\ell_n U_\ell + \sqrt{\ell(\ell+1)}{}_nV_\ell\right] \mathrm{d}r, \tag{73}$$

$$l_\ell(r) = -g \sum_{n=0}^{\infty} \frac{{}_nV_\ell(r)}{{}_n\omega_\ell^2} \times \int_0^a \rho \frac{r^{\ell+1}}{a_\ell} \left[\ell_n U_\ell + \sqrt{\ell(\ell+1)}{}_nV_\ell\right] \mathrm{d}r/\sqrt{\ell(\ell+1)}. \tag{74}$$

Note that in the case of the $(2\ell + 1)$-degenerate SNREI model, we drop m when referring to modes (${}_n\mathcal{S}_\ell$) and eigenfunctions (${}_nU_\ell$ and ${}_nV_\ell$). Fig. 3(a) shows the calculation of static Love numbers at $r = a$ based on both our normal mode approach (eqs 73 and 74) and the formalism of Farrell (1972) as a function of spherical harmonic degree using the SNREI version of the model PREM (Dziewonski & Anderson 1981). The agreement is excellent.

The advantage of the normal mode approach relative to classic Love number theory is that it allows examination of the contribution from each mode and this provides insight into the physics and sensitivity of the associated response. If we consider the semi-diurnal tide case, the forcing is limited to $\ell = 2$ and $m = 2$ and the response of an SNREI Earth involves the same degree and order. Fig. 3(b) partitions the h_2 Love number into contributions from each overtone n, demonstrating that the ${}_0\mathcal{S}_2$ mode contributes ~ 95 per cent of the response. It is worth noting that not all normal mode contributions to h_2 will have the same sign, since a given mode's contribution will depend upon both the degree of excitation and the manner in which the mode samples the Earth. This is evident from the results for ${}_3\mathcal{S}_2$ (or $n = 3$) in Fig. 3(b), which has a contribution of opposite sign to the other modes. It is clear that, within the limits of observation, the summation in eq. (73) can safely be truncated by $n \sim 10$, making any tidal calculation computationally inexpensive.

Fig. 4 shows the depth sensitivity kernels for the relative shift in eigenfrequency of each mode (for n up to 4) for density and two seismic velocities, v_p and v_s, which are the three parameters most commonly discussed in the seismic problem (expressions for these kernels may be found in Dahlen & Tromp 1998). For the most important parameter in the geodynamics problem, the mass density ρ, ${}_0\mathcal{S}_2$ has the most sensitivity in the lower mantle. Each overtone shown in Fig. 4 has differing depth sensitivities. Perhaps the most striking example is ${}_2\mathcal{S}_2$, which has no sensitivity in the mantle or most of the outer core; its main sensitivities are limited to inner core boundary and within the inner core. These simple examples illustrate the fundamental connection between the Earth's free oscillations, for the earthquake response, and forced oscillations, for the tidal response.

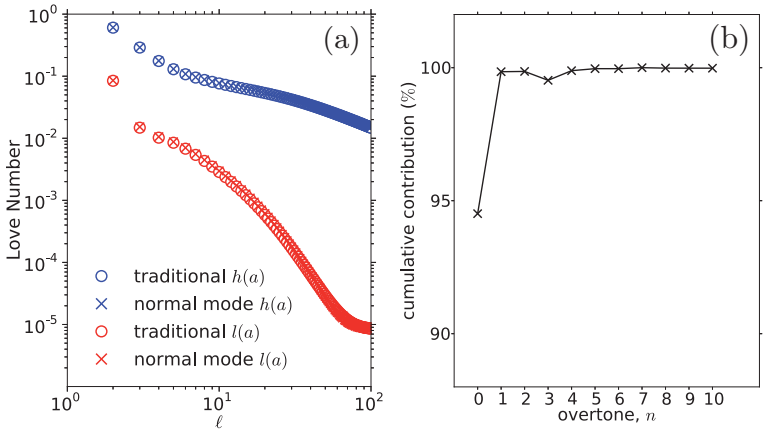

Figure 3. (a) Tidal Love numbers evaluated at $r = a$ for the SNREI version of PREM (Dziewonski & Anderson 1981) using traditional Love number theory (◯) and normal mode theory (×). The h_ℓ Love number (blue) is associated with radial displacement and the l_ℓ Love number (red) relates to tangential displacement. (b) Contribution of each ${}_n\mathcal{S}_2$ mode towards the $h_2(a)$ Love number. See the summation in eq. (73).

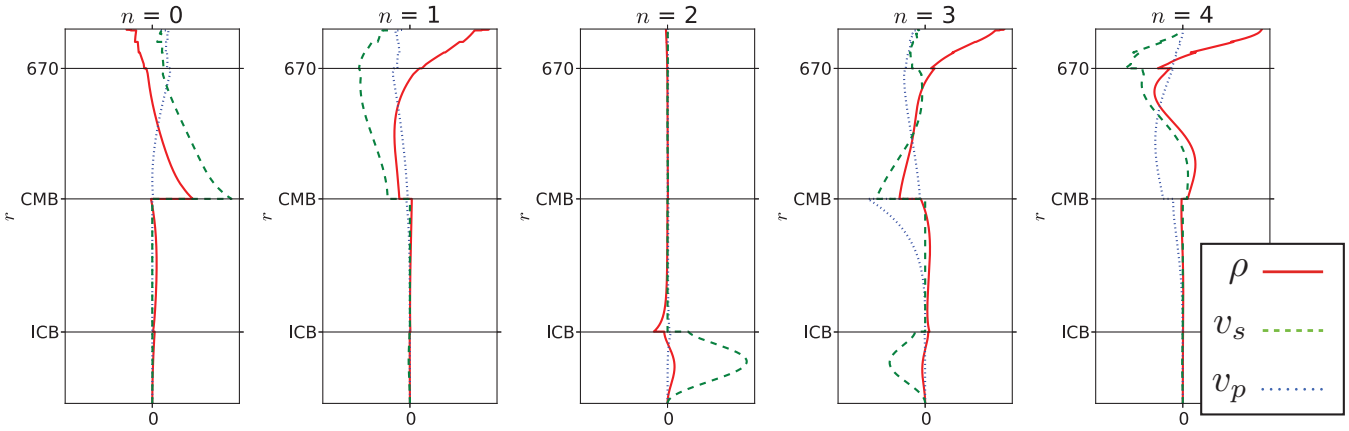

Figure 4. Depth-dependent sensitivity kernels for the ${}_n\mathcal{S}_2$ set of modes. Red solid line: density, ρ; green dashed line: shear velocity, v_s; blue dotted line: compressional velocity, v_p. All curves are normalized such that, in each panel, only relative values are of importance.

3.1.2 Anelastic Earth

In the following, we present some numerical predictions using a simple anelastic Earth model designed to demonstrate the theory presented in Section 2.4. To simplify the discussion, we set $\mathbf{\Omega} \to \mathbf{0}$, which results in $\mathbf{W} \to \mathbf{0}$ in eq. (27). [Thus, only the real Earth needs to be solved for. In this case, the normalizations change, but we need only to substitute $\overline{\boldsymbol{\chi}}$ for $\boldsymbol{\chi}$ in eq. (33).] We also assume that the Earth's rheology may be modelled as a single standard linear solid using simple piecewise-constant depth dependence. Adopting such a simple Earth model avoids a contribution to the response from branch cuts, although our theory is fully capable of incorporating such complexity.

The 1-D mechanical analogue for this Earth model is shown in Fig. 5(a), where we take the unrelaxed limit (μ_0) to be that of PREM, and μ_1 to be $20 \times \mu_0$ in the upper mantle and $50 \times \mu_0$ in the lower mantle. The viscosity, η, is $\tau\mu_1$ where we set τ, the characteristic timescale, to be 10 hr. We choose τ to lie significantly beyond the seismic band to highlight the necessity of searching for relaxation modes outside this band. In general, the Earth model parameters have been chosen to yield a modulus reduction similar to that predicted by the PREM Q model across the seismic band. We assume no dissipation in κ.

Following Nowick & Berry (1972), the frequency dependence of μ becomes

$$\mu(\nu) = \mu_0 - \frac{\delta\mu}{1 + i\nu\tau_\epsilon}, \tag{75}$$

where

$$\delta\mu = \mu_0 \left(1 - \frac{\mu_1}{\mu_0 + \mu_1}\right). \tag{76}$$

There are two characteristic timescales, τ_ϵ and τ_σ, where

$$\tau_\epsilon = \frac{\eta}{\mu_0 + \mu_1}, \tag{77}$$

$$\tau_\sigma = \frac{\eta}{\mu_1}. \tag{78}$$

As described in Section 2.4, we expect the elastic eigenfrequency to be perturbed by $\delta\omega_k$ due to the reduction in the shear modulus (see eq. 75). The imaginary perturbation γ_k will be due to Q_k, where from eq. (19) the Q of a standard linear solid is given by

$$Q_\mu^{-1}(\omega) = \frac{\omega(\tau_\sigma - \tau_\epsilon)}{1 + \omega^2\tau_\sigma\tau_\epsilon}. \tag{79}$$

This form is a Debye peak centred around $\sqrt{\tau_\epsilon\tau_\sigma}$ (Zener 1948).

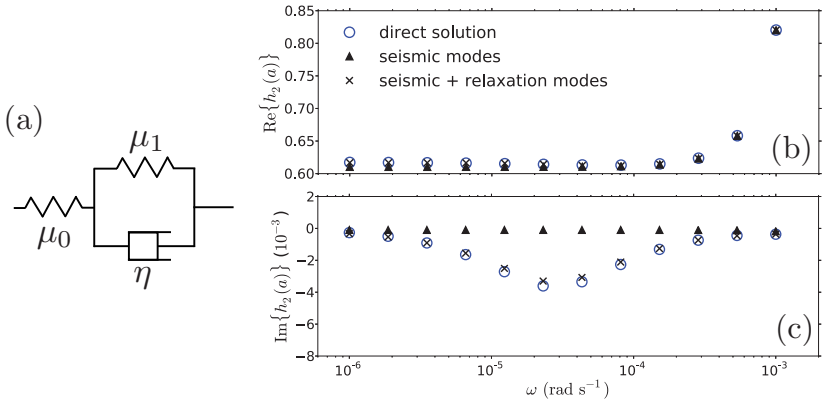

Figure 5. (a) A schematic illustration of a standard linear solid (or Zener solid; Zener 1948) composed of two mechanical springs (μ_0, μ_1) and one dashpot (η). (b) The real part of the $h_2(r = a)$ Love number across different frequencies computed using two methods: the direct solution method (blue) and the normal mode method (black). (c) The same as (b), except for the imaginary part of $h_2(r = a)$.

In considering the anelastic eigenfunction in this numerical example, we apply one simplification relative to the theory described in Section 2.4; namely, we ignore anelastic cross-coupling and consider only self-coupling. For a spherically symmetric Earth, modes are $(2\ell + 1)$-degenerate and only overtones of the same degree couple. In the body tide case, ignoring cross-coupling is an excellent assumption that avoids the necessity of solving the eigenvalue problem defined by eq. (27). To achieve this, we set all off-diagonal components for $\mathbf{V}$ to zero and in this case the matrix with elements $V_{kk'}$ reduces to a vector with elements V_k, where

$$V_k \approx 2i\omega_k\gamma_k. \tag{80}$$

Similarly, using eq. (33), $\chi_{kk'}$ reduces to χ_k, where

$$\chi_k^2 \approx \left[1 - \frac{1}{2\nu_k}\partial_\nu V_k(\nu)\right]^{-1}, \tag{81}$$

leaving the anelastic eigenfunction

$$\mathbf{s}_k = \chi_k \mathbf{s}_k^e. \tag{82}$$

Finally, we also search for modes along the imaginary axis, the so-called relaxation modes (see Fig. 1). Once the anelastic eigenfrequencies and eigenfunctions are found, we perform the convolution in eq. (55), where $\mathbf{B} = \mathbf{0}$, using the version of the Green's function given by eq. (53).

To investigate the importance of the relaxation modes in modelling the tidal response we use the normal mode theory described in Section 2.4 and above to calculate the Love number $h_2(a)$ over a frequency range spanning three orders of magnitude in period, from ∼2 hr to 100 d. In Figs 5(b) and (c), we compare results in the cases where the relaxation modes are included, or not included, in the normal mode summation. We also compare these results to predictions generated using a direct solution approach (Hara *et al.* 1993; Al-Attar 2007). The direct solution method solves the forced equation (eq. 3) and does not involve a summation of the anelastic eigenfunctions and eigenfrequencies, and it thus serves as an independent check on our normal mode treatment of the tidal problem. The lowest frequency seismic mode, ${}_0\mathcal{S}_2$, has an eigenfrequency of approximately 1 hr^{-1}. Thus, the set of seismic modes will not capture any anelastic processes at periods greater than about 1 hr. Since our rheological (standard linear solid) model has an attenuation that peaks near 10 hr, the normal mode expansion that includes only the seismic modes is insufficient to accurately predict the impact of anelasticity on the tidal response. In contrast, the calculation based on the full set of (seismic plus relaxation) modes accurately reproduces the response computed using the direct solution method.

In the seismic literature, mode catalogues are often displayed using the so-called dispersion diagrams. Fig. 6 shows a dispersion diagram that includes low-frequency seismic modes together with an analogue for the case of the relaxation modes that is often adopted in studies of glacial isostatic adjustment. Fig. 6(a) shows both $\mathrm{Re}\{\nu_k\}$ and $\mathrm{Im}\{\nu_k\}$ for the seismic modes (orange-scale triangles), where the former represent frequencies of oscillation and the latter are inverse decay times. Note that these two sets of orange-scale data points (dashed and solid lines) are from a single set of modes. The inverse decay times for the relaxation modes (blue-scale circles) are shown with a smaller frequency range in Fig. 6(b). As expected, given the adopted viscosity structure of the standard linear solid, the inverse decay times all cluster around 10 hr. The colour scale indicates the contribution of each mode to the long-term h_2 Love number. As in Fig. 3(b), the contribution of the fundamental seismic mode to the tidal response is greatest in all cases.

3.2 Aspherical Earth

All tests described in this section are performed with elastic and isotropic Earth models. Our normal mode methodology and the finite-volume scheme are hereafter referred to as NM and FV, respectively. The FV method computes the deformation of a non-rotating and self-gravitating Earth in response to a body force (Latychev 2005; Latychev *et al.* 2009). The governing equations are discretized on a tetrahedral grid within a spherical domain that incorporates arbitrary variability in crustal/mantle elastic and density structure. Latychev *et al.* (2009) used the FV scheme to predict the body tides on an aspherical Earth model, and we use it for the same purpose in several of the tests summarized below.

Since we only consider elastic models, we need only calculate the response to a single time step of forcing. In all tests, we apply a semi-diurnal tidal potential using the form given in eq. (1), where $c_{\ell m}$ is

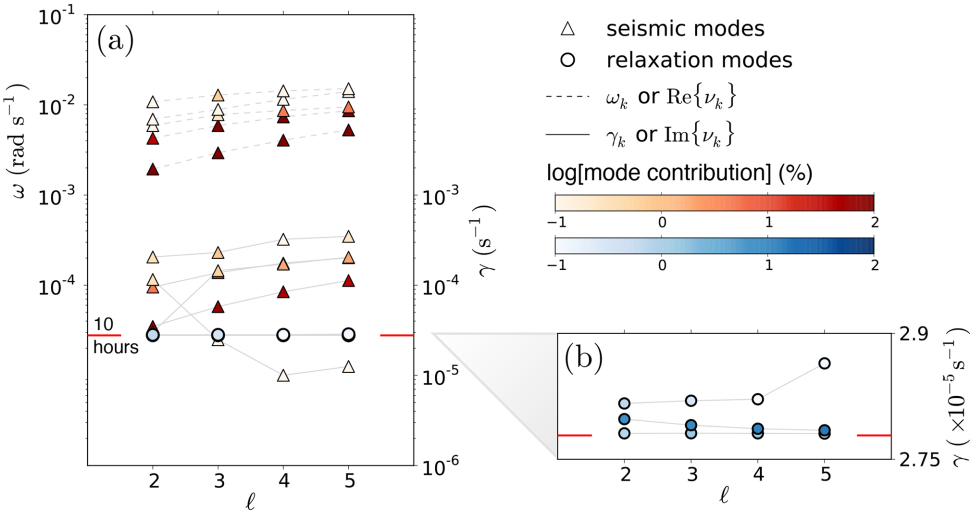

Figure 6. (a) The left vertical axis shows the real part of ν_k (oscillatory frequencies). The right vertical axis shows the imaginary part of ν_k (inverse decay times). The orange symbols denote seismic modes while the blue symbols are relaxation modes. The grey lines connect modes of equivalent overtone, n, where dashed (solid) lines are for the real (imaginary) part of eigenfrequencies. The colour intensity indicates each mode's contribution to the long-term Love number. (b) A zoomed-in version of (a) focusing only on relaxation modes.

only non-zero for $\ell = 2$ and $m = \pm 2$. Recall that the $Y_{\ell m}$ spherical harmonic is complex and normalized as defined by Edmonds (1960), as discussed in Section 2.1. We set $c_{2\pm 2} = 5.5$, which leads to a maximum radial crustal displacement of 25 cm, typical for a semi-diurnal tide associated with a lunar potential forcing. If we denote the radial displacement response at the surface of the perturbed Earth model due to the tidal forcing by $s_r(\theta, \lambda)$, then a spherical harmonic decomposition of the response is given by:

$$s_r(\theta, \lambda) = \sum_{\ell=0}^{\infty} \sum_{m=-\ell}^{\ell} S_{\ell,m} Y_{\ell m}(\theta, \lambda). \tag{83}$$

3.2.1 Aspherical structure

In the NM method, aspherical perturbations in Earth structure lead to mode coupling. As discussed in Section 2.5, the perturbations are expanded in spherical harmonics and they are incorporated into the perturbation matrices $\mathbf{T}$ and $\mathbf{V}'$ (Woodhouse 1980). In this section, we focus only on spheroidal modes (and radial displacement) and we consider the modes listed in the right column of Table 2. We note that our theory is fully capable of considering toroidal–toroidal and toroidal–spheroidal coupling. Let us define a perturbation in structure of degree s and order t by the shorthand notation $\{s, t\}$.

Let us also consider a mode k of degree and order $\{\ell, m\}_k$ and overtone n, and a mode k' of degree and order $\{\ell', m'\}_{k'}$ and overtone n'. For clarity, we include the subscripts k and k' in reference to these modes. The two modes will couple with the $\{s, t\}$ structure in a manner that satisfies the following selection rules:

$$m + m' + t = 0, \tag{84}$$

$$|\ell - \ell'| \leq s \leq |\ell + \ell'|, \tag{85}$$

$$\ell' + \ell + s = \text{even}, \tag{86}$$

that are governed by the so-called 3-j triangle condition (in Section 2.5 we symbolically represented these conditions using the variable ζ). Note that the overtones n and n' do not play a role in these selection rules. Seismic normal mode perturbation theory accounts for both direct coupling and indirect coupling. That is to say, in the unperturbed problem, a body force of degree ℓ and order m will only excite a mode of the same ℓ and m. A perturbation of structure with the form $\{s, t\}$ will also allow this mode to couple to modes of different degree ℓ' and order m'. This coupling is illustrated by Fig. 2 where if mode 'A' has the same ℓ and m of the forcing, the off-diagonal matrices (shaded green) would be the result of direct coupling. These coupled modes will, in turn, indirectly couple, though weakly, to other modes in the presence of $\{s, t\}$ structure, under the same selection rules, so long as the modes are included in matrices $\mathbf{T}$ and $\mathbf{V}'$. In the terminology of Qin *et al.* (2014), direct coupling would be equivalent to first-order coupling and indirect coupling includes all higher order couplings.

In this section, we describe two tests that involve idealized perturbations to the spherically symmetric, non-rotating, elastic and isotropic (SNREI) version of the Earth model PREM (Dziewonski & Anderson 1981). The perturbations are constant throughout the mantle. That is, an $\{s, t\}$ perturbation to the density field is applied to every layer in the mantle and has the following spatial dependence:

$$\rho(\theta, \lambda, r) = \rho^0(r)\left[1 + \epsilon Y_{st}(\theta, \lambda)\right], \tag{87}$$

where ϵ is an arbitrary scaling factor.

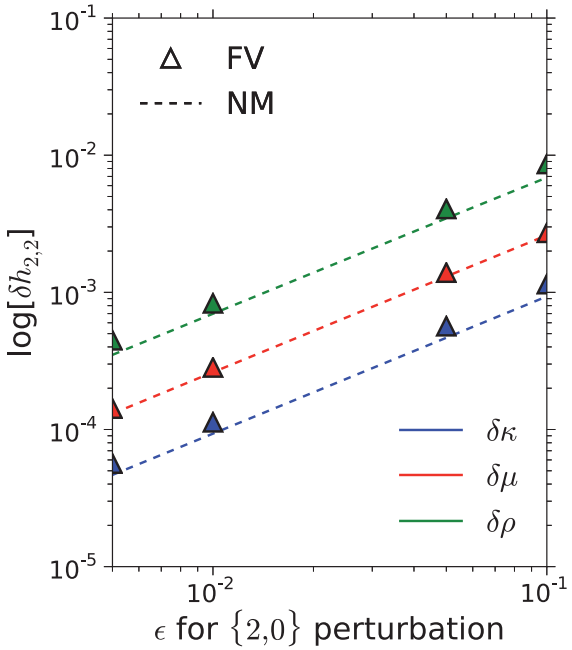

Figure 7. Benchmark comparison of results based on a finite volume ('FV') code (Latychev *et al.* 2009) and the normal mode perturbation theory ('NM') described in the text. A $c_{2,2}$ body force is applied to an Earth model with imposed $\{2, 0\}$ structure of varying amplitude, where the latter is governed by the parameter ϵ (eq. 87). The figure shows the perturbation $\delta h_{2,2}$ (eq. 90) from results computed using SNREI PREM structure.

If $\epsilon = 0$ (i.e. a spherically symmetric or reference Earth model), then the spherically symmetric h_2^0 Love number is defined as

$$S_{2,2}^0 = \frac{h_2^0}{g} c_{22}. \tag{88}$$

In this special case, the Love number is independent of order.

In our first test, we impose a degree 2 and order 0 (i.e. $\{s, t\} = \{2, 0\}$) lateral perturbation to the 1-D profile of ρ (as in eq. 87) for scaling factors ϵ ranging from 0.005 to 0.1. This range is equivalent to a maximum perturbation in the density of 0.03–6.3 per cent. In this case, we generalize the above expression defining the Love number to be

$$S_{2,2} = \frac{h_{2,2}(\epsilon)}{g} c_{22} \tag{89}$$

and the associated perturbation to the Love number as

$$\delta h_{2,2}(\epsilon) = h_{2,2}(\epsilon) - h_2^0. \tag{90}$$

In Fig. 7, we show our normal mode calculation of $\delta h_{2,2}$ as a function of ϵ (green dashed line); the solid green triangles are calculations based on the FV scheme. We repeat all these calculations for independent perturbations in the shear and bulk moduli and the results are shown in red and blue, respectively. The results generated from the NM and FV calculations are in excellent agreement.

Next, we prescribe a perturbation in the shear velocity (v_s) structure of the mantle. We consider the three cases listed in Table 1. In the first, we adopt a scaling factor (which we denote by ϵ_{v_s}) of 0.001 and an aspherical perturbation from the spherically symmetric structure of spherical harmonic degree 3 and order 1 ($\{3, 1\}$). The next case adopts $\epsilon_{v_s} = 0.01$ and $\{2, 2\}$, and the final case has $\epsilon_{v_s} = 0.1$ and $\{1, 1\}$. In each case, we use the following scaling relations to convert the shear velocity perturbation to perturbations

Table 1. The aspherical perturbation in Earth structure ($\{s, t\}$) and its amplitude, as prescribed by the parameter ϵ_{v_s}, for the second set of tests described in Section 3.2.1.

$\{s, t\}$	ϵ_{v_s}
$\{3, 1\}$	0.001
$\{2, 2\}$	0.01
$\{1, 1\}$	0.1

Table 2. Spheroidal mode coupling for the group and the full coupling methods, capped at a maximum degree of 6, adopted in the test described in Section 3.2.2. The group coupling calculation considers six distinct groups whereas the full coupling calculation considers one single group with 30 modes.

Group coupling	Full coupling
${}_0\mathcal{S}_2$	${}_0\mathcal{S}_2{-}{}_2\mathcal{S}_1{-}{}_0\mathcal{S}_3{-}{}_0\mathcal{S}_4{-}{}_1\mathcal{S}_2{-}$
${}_0\mathcal{S}_4{-}{}_1\mathcal{S}_2$	${}_0\mathcal{S}_0{-}{}_0\mathcal{S}_5{-}{}_1\mathcal{S}_3{-}{}_2\mathcal{S}_2{-}{}_3\mathcal{S}_1{-}$
${}_2\mathcal{S}_2$	${}_0\mathcal{S}_6{-}{}_3\mathcal{S}_2{-}{}_1\mathcal{S}_4{-}{}_2\mathcal{S}_3{-}{}_1\mathcal{S}_5{-}$
${}_3\mathcal{S}_2$	${}_2\mathcal{S}_4{-}{}_4\mathcal{S}_1{-}{}_4\mathcal{S}_1{-}{}_3\mathcal{S}_3{-}{}_2\mathcal{S}_5{-}$
${}_5\mathcal{S}_1{-}{}_4\mathcal{S}_2$	${}_1\mathcal{S}_6{-}{}_1\mathcal{S}_0{-}{}_2\mathcal{S}_6{-}{}_5\mathcal{S}_1{-}{}_4\mathcal{S}_2{-}$
${}_5\mathcal{S}_2$	${}_3\mathcal{S}_4{-}{}_6\mathcal{S}_1{-}{}_4\mathcal{S}_3{-}{}_2\mathcal{S}_5{-}{}_3\mathcal{S}_5$

in elastic moduli and density structure:

$$\frac{\partial \ln v_s}{\partial \ln \rho} = 0.4, \tag{91}$$

$$\frac{\partial \ln v_s}{\partial \ln \mu} = 2.4, \tag{92}$$

$$\frac{\partial \ln v_s}{\partial \ln \kappa} = 0.5. \tag{93}$$

These are plausible values in the simple case of constant mantle scaling (Bolton 1996).

Fig. 8 summarizes the results as a spherical harmonic decomposition of the total radial displacement response up to degree and order 6. We note that this figure provides no information in regard to the contributions of each overtone to the spatial signal $S_{\ell,m}$; the overtones we included in the calculation are listed in the right column of Table 2. The figures to the left were computed using the FV numerical scheme, while those on the right were computed using our NM approach. The match is excellent (note the log scale); discrepancies between predictions of displacement based on the NM and FV methods are significantly below the per cent level. Benchmark tests in the case of the surface mass loading problem (Latychev 2005) suggest numerical noise in the FV calculations on the order of several parts in 1000 and we conclude that the discrepancies that exist in Fig. 8 primarily reflect numerical error in the FV method.

The results in Fig. 8 largely reflect the selection rules described above. Consider, as an example, Fig. 8(f). The imposed perturbation in structure is $\{2, 2\}$ and, given the applied $c_{2,2}$ tidal potential, the geometry of the primary mode k to be excited is $\{2, 2\}_k$. Substituting harmonics governing the aspherical structure and forcing into the 3-j triangle condition yield the selection rules:

$$\pm 2 + m' \pm 2 = 0, \tag{94}$$

$$|2 - \ell'| \leq 2 \leq |2 + \ell'|, \tag{95}$$

$$\ell' + 2 + 2 = \text{even}. \tag{96}$$

Modes that satisfy all these conditions are $\{0, 0\}_{k'}$, $\{2, 0\}_{k'}$, $\{2, \pm 2\}_{k'}$, $\{4, 0\}_{k'}$, $\{4, \pm 4\}_{k'}$; which are excited as a result of 'direct coupling'. These modes, in turn, couple to other modes, though this 'indirect coupling' tends to be weak. In the case of Fig. 8(f), this indirect coupling is evident in the excitation of $\{6, \pm 6\}_{k'}$. Substituting the harmonic $\{4, \pm 4\}_k$ as mode k in the 3-j triangle condition predicts that a $\{6, \pm 6\}_{k'}$ mode will be excited, though this excitation is weak (Fig. 8f). A similar discussion of the relevant selection rules recovers the response geometry evident in Figs 8(b) and (d).

We note that harmonics in the FV response on the left column of Fig. 8 show power at some degrees and orders that violate the above selection rules, and this supports our assertion that differences in the FV and NM largely reflect numerical errors in the former.

3.2.2 *Group coupling versus full coupling*

To reduce computational complexity in studies of the Earth's seismic free oscillations, a method known as the quasi-degenerate or group coupling approximation may be employed (e.g. Resovsky & Ritzwoller 1995). In this method, eigenmodes whose spherically symmetric eigenfrequencies lie close together are grouped and assigned a fiducial frequency, ω_f, often taken to be the average of the eigenfrequencies. Then, rather than solving for all the eigenfrequencies of the system, as is required in the eigenvalue problems defined by eqs (46) and (47) (i.e. the full coupling calculation), first-order perturbations to the fiducial frequencies, $\delta\omega$, are found. This approach reduces the quadratic eigenvalue problem (eqs 46 and 47), which involves one large, full coupling matrix, to an ordinary eigenvalue problem for each grouping of modes, and thus it involves matrices of much smaller dimension (Dahlen & Tromp 1998). Solutions to the latter yield the perturbations $\delta\omega$.

The assumption inherent to group coupling is that within a group $\delta\omega \ll \omega_f$. Although group coupling has been used in seismic applications in the past, the accuracy of the method has been challenged (Deuss & Woodhouse 2001). To consider the relative accuracy of these methods in the case of the body tide problem, we compare predictions generated using full and group coupling for an Earth model with aspherical structure. In particular, we impose density and elastic structure in the mantle by scaling shear wave velocity model S20RTS (Ritsema *et al.* 1999), using eqs (91)–(93). We calculate δs_r by applying the same tidal potential as in previous tests (see Section 3.2.1). Table 2 lists the six groups of modes adopted for the group coupling calculation and also the complete set of 30 modes in the full coupling case. There are clearly far fewer modes included in the former due to the restrictions on the frequency range of each group. Note that each of these groups must contain at least one ${}_n\mathcal{S}_2$ mode in order to be excited by the tidal force.

Figs 9(a) and (b) provide maps of the difference in radial displacement (δs_r) between the aspherical and reference (spherically symmetric) cases for both group (left) and full (right) coupling applications of the NM methodology. The predictions are markedly different, with the group coupling case showing little excitation of modes for $\ell \neq 2$ (see Figs 9c and d). In the full coupling calculation, the dominant coupling produces large $S_{4,4}$ and $S_{2,0}$ signals in the displacement response. All other signals associated with coupling are at least an order of magnitude lower (Fig. 9d).

There is a fundamental difference between the nature of an earthquake source, involving an impulse forcing with a variety of spatial and temporal harmonics exciting a wide range of eigenmodes, versus a tidal source, a body force that acts through the whole Earth

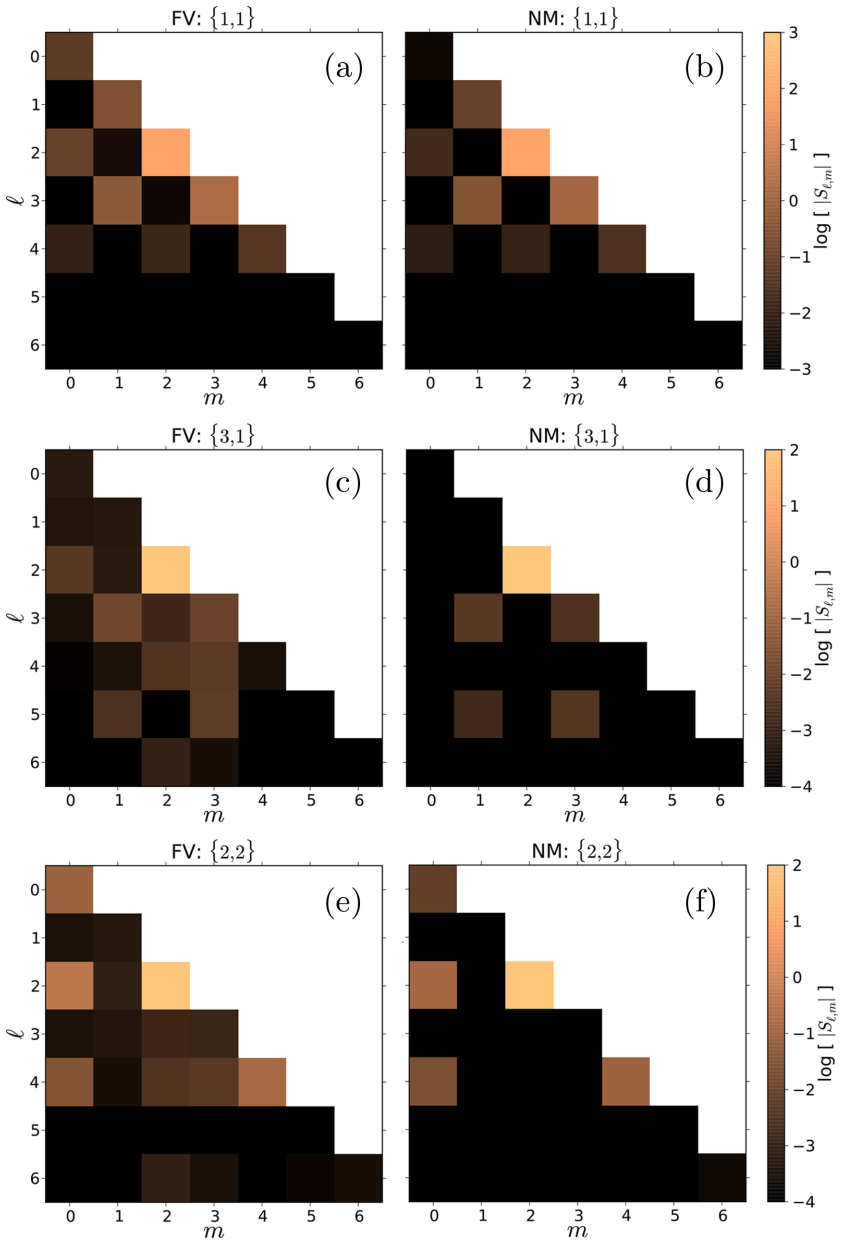

Figure 8. Benchmark comparison of results based on (left panels) a finite volume ('FV') code (Latychev *et al.* 2009) and (right panels) the normal mode perturbation theory ('NM') described in the text. A $c_{2,2}$ body force is prescribed with three different idealized aspherical elastic mantle structures of the form $\{s, t\}$ (see Section 3.2.1 for details). The predictions in each case are decomposed in terms of spherical harmonic coefficients $S_{\ell,\,m}$.

within narrow frequency bands and a single spatial wavelength. This difference has clear implications for mode coupling and we conclude, on the basis of Fig. 9, that full coupling must always be applied when a normal mode methodology is adopted to calculate the impact of aspherical Earth structure on the Earth's body tide response.

3.2.3 Rotation

Earth rotation will perturb the body tide response relative to a non-rotating model and will lead to a response at degrees $\ell \neq 2$ (Wahr 1981b; Dehant 1987; Wang 1994). Within the NM method, this perturbation arises through coupling of modes and is accounted for by two aspects of the underlying theory: first, by the presence of the Coriolis matrix, **W** (eq. 44); and second, by components of the matrices **T** and **V**′ that account for both the ellipticity of the Earth, which is an aspherical perturbation in Earth structure of $\{2, 0\}$ geometry, and the centrifugal potential energy (Dahlen 1968).

The impact of rotation is characterized by a specific splitting and coupling of modes. In the case of an elastic Earth with no aspherical structure other than a rotation-induced ellipticity, a mode k will couple with: (i) a mode of like ℓ and m; (ii) a mode k' where $m' = m$ and $\ell' = \ell \pm 2$; and (iii) a toroidal mode of $\ell' = \ell \pm 1$ (due to the Coriolis operator; this final coupling is very minor and we do not discuss it further). For a semi-diurnal forcing, this coupling would lead to a response, as expressed by the spherical harmonic expansion (eq. 83), that has only non-zero components of $S_{2,\,2}$ and $S_{4,\,2}$. We have found that the perturbations from the reference (non-rotating) case for components $S_{2,\,2}$ and $S_{4,\,2}$ are $+0.05$ and -0.01 per cent, respectively, of the reference value, $S^0_{2,2}$.

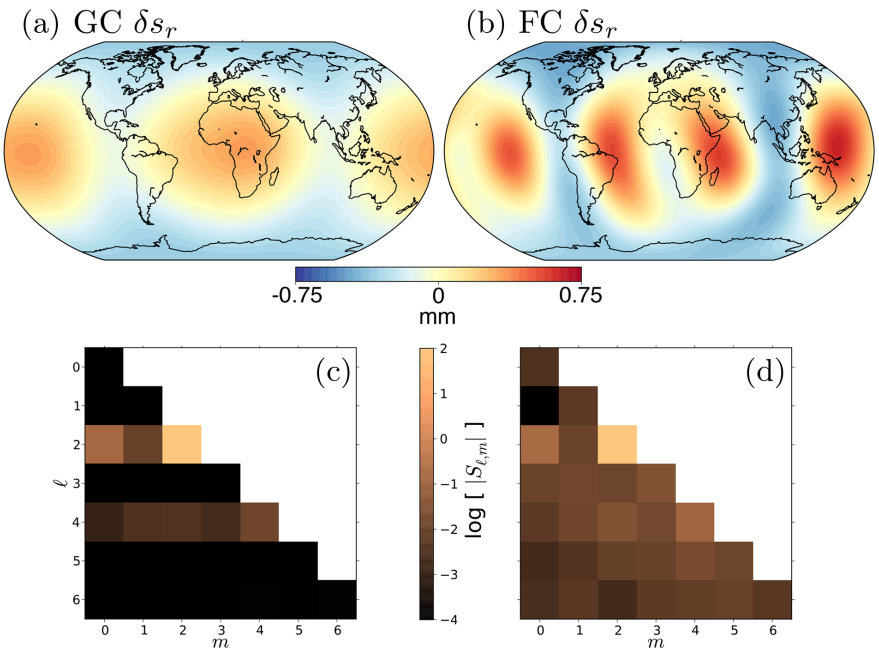

Figure 9. The radial displacement of an elastic, aspherical Earth with imposed S20RTS (Ritsema *et al.* 1999) structure (with scaling factors given by eqs 91–93) in response to a $c_{2,2}$ body force. (a, b) The residual field, δs_r, using the group and the full coupling methods, respectively. (c, d) The spherical harmonic decomposition of the total radial displacement response computed using the group and the full coupling methods, respectively.

4 SUMMARY

We have derived a theoretical framework for predicting the semi-diurnal and long-period body tides on an aspherical, rotating and anelastic Earth that is based on seismic free oscillation theory. As we have discussed, in the most general form the problem involves a non-Hermitian operator which can be solved by introducing a dual space (Lognonné 1991). We have also described a generalized normal mode treatment of the impact of anelasticity on the body tide response. While based on free oscillation theory, our treatment is distinct from the approach used in seismic applications. It is also distinct from the theory developed by Wahr & Bergen (1986) to incorporate anelastic effects. In the context of our theory, accurately capturing the impact of anelastic effects requires that relaxation modes outside the usual seismic band be included in the normal mode summation.

We have presented some simple numerical calculations that demonstrate that classical Love number results (Farrell 1972) for an SNREI Earth can be reproduced using the normal mode framework. These calculations highlight the physics of the tidal response as well as its sensitivity to Earth structure, as reflected by sensitivity kernels.

We have also outlined a perturbation scheme, taken from the seismic free oscillation literature to compute the impact on body tide displacements of lateral variations in Earth structure. We performed a series of tests using the NM methodology and benchmarked the results against calculations based on a fully numerical, FV methodology (Latychev *et al.* 2009). Our main conclusion is that the impact of aspherical structure on the body tide response must be based on a full coupling of eigenmodes rather than group coupling, which is in agreement with previous normal mode studies (Deuss & Woodhouse 2001). While full coupling is computationally expensive in the seismic problem, the limited spectral range of the tidal forcing and response makes it easily tractable for body tide calculations and thus the implementation of full coupling does not pose any practical difficulty. Differences between predictions based on the NM and FV methodologies were significantly below the per cent level, and it is likely that these differences originate from numerical inaccuracies in the FV scheme.

In future work, we will elaborate on our new normal mode treatment of anelasticity and discuss the implications of the method for interpreting measurements of anelastic effects on body tides (e.g. phase lags) and for inferring Earth structure. Ultimately, our goal is to combine our generalized treatment of semi-diurnal and long-period body tides on an aspherical, rotating and anelastic Earth, with space-geodetic and long-period seismic measurements, to perform the first global tomographic tidal analysis of the Earth's long-wavelength elastic and density structure.

ACKNOWLEDGEMENTS

We thank John Wahr and an anonymous reviewer for their comprehensive and constructive comments on earlier versions of this manuscript which led to a number of important improvements. This work was supported by funding from Harvard University (HL, JXM), the National Science Council of Taiwan grants 102-2917-I-564-063 and 103-2811-M-002-223 (H-YY), and the Canadian Institute for Advanced Research (KL, JXM).

REFERENCES

Agnew, D., 2007. *Treatise on Geophysics,* Elsevier.

Al-Attar, D., 2007. A solution of the elastodynamic equation in an anelastic earth model, *Geophys. J. Int.,* **171**(2), 755–760.

Alterman, Z., Jarosch, H. & Pekeris, C.L., 1959. Oscillations of the Earth, *Proc. R. Soc. A,* **252**(1268), 80–95.

Anderson, D.L. & Minster, J.B., 1979. The frequency dependence of Q in the Earth and implications for mantle rheology and Chandler wobble, *Geophys. J. Int.,* **58**(2), 431–440.

Benjamin, D., Wahr, J., Ray, R.D., Egbert, G.D. & Desai, S.D., 2006. Constraints on mantle anelasticity from geodetic observations, and implications for the J_2 anomaly, *Geophys. J. Int.,* **165**(1), 3–16.

Bolton, H., 1996. Long period travel times and the structure of the mantle, *PhD thesis,* University of California, San Diego.

Cartwright, D.E. & Edden, A.C., 1973. Corrected tables of tidal harmonics, *Geophys. J. Int.,* **33**(3), 253–264.

Dahlen, F.A., 1968. The normal-modes of a rotating, elliptical Earth, *Geophys. J. Int.,* **16**(4), 329–367.

Dahlen, F.A., 1972. Elastic velocity anisotropy in the presence of an anisotropic initial stress, *Bull. seism. Soc. Am.,* **62**(5), 1183–1193.

Dahlen, F.A. & Tromp, J., 1998. *Theoretical Global Seismology,* Princeton University Press.

Dehant, V., 1987. Tidal parameters for an inelastic Earth, *Phys. Earth planet. Inter.,* **49**(1–2), 97–116.

Dehant, V., Defraigne, P. & Wahr, J.M., 1999. Tides for a convective Earth, *J. geophys. Res.,* **104**(B1), 1035–1058.

Deuss, A. & Woodhouse, J., 2004. Iteration method to determine the eigenvalues and eigenvectors of a target multiplet including full mode coupling, *Geophys. J. Int.,* **159**(1), 326–332.

Deuss, A. & Woodhouse, J.H., 2001. Theoretical free-oscillation spectra: the importance of wide band-coupling, *Geophys. J. Int.,* **146**(3), 833–842.

Dziewonski, A.M. & Anderson, D.L., 1981. Preliminary reference Earth model, *Phys. Earth planet. Inter.,* **25**(4), 297–356.

Edmonds, A.R., 1960. *Angular Momentum in Quantum Mechanics,* Princeton University Press.

Farrell, W.E., 1972. Deformation of the Earth by surface loads, *Rev. Geophys.,* **10**(3), 761–797.

Gilbert, F., 1970. Excitation of the normal modes of the Earth by earthquake sources, *Geophys. J. Int.,* **22**(2), 223–226.

Hara, T., Tsuboi, S. & Geller, R.J., 1993. Inversion for laterally heterogeneous upper mantle S-wave velocity structure using iterative waveform inversion, *Geophys. J. Int.,* **115**(3), 667–698.

Herring, T.A. & Dong, D., 1994. Measurement of diurnal and semi-diurnal rotational variations and tidal parameters of Earth, *J. geophys. Res.,* **99**(B9), 18 051–18 071.

Ito, T. & Simons, M., 2011. Probing asthenospheric density, temperature, and elastic moduli below the western United States., *Science,* **332**(6032), 947–951.

Jackson, I., Fitzgerald, J.D., Faul, U.H. & Tan, B.H., 2002. Grain-size-sensitive seismic wave attenuation in polycrystalline olivine, *J. geophys. Res.,* **107**(B12), 2360, doi:10.1029/2001JB001225.

Kanamori, H. & Anderson, D.L., 1977. Importance of physical dispersion in surface wave and free oscillation problems: review, *Rev. Geophys. Space Phys.,* **15**(1), 105–112.

Kim, T.-H. & Shibuya, K., 2013. Verification of the ellipsoidal earth model with an inelastic and convective mantle using tidal gravity variations revisited, *Geophys. J. Int.,* **194**(1), 230–248.

Krásná, H., Böhm, J. & Schuh, H., 2013. Tidal Love and Shida numbers estimated by geodetic VLBI, *J. Geodyn.,* **70,** 21–27.

Latychev, K., 2005. Influence of lithospheric thickness variations on 3-D crustal velocities due to glacial isostatic adjustment, *Geophys. Res. Lett.,* **32**(1), L01304, doi:10.1029/2004GL021454.

Latychev, K., Mitrovica, J.X., Ishii, M., Chan, N.-H. & Davis, J.L., 2009. Body tides on a 3-D elastic Earth: toward a tidal tomography, *Earth planet. Sci. Lett.,* **277**(1–2), 86–90.

Lekić, V., Matas, J., Panning, M. & Romanowicz, B., 2009. Measurement and implications of frequency dependence of attenuation, *Earth planet. Sci. Lett.,* **282**(1–4), 285–293.

Liu, H.-P., Anderson, D.L. & Kanamori, H., 1976. Velocity dispersion due to anelasticity; implications for seismology and mantle composition, *Geophys. J. Int.,* **47**(1), 41–58.

Lognonné, P., 1991. Normal modes and seismograms in an anelastic rotating Earth, *J. geophys. Res.,* **96**(B12), 20 309–20 319.

Love, A.E.H., 1911. *Some Problems of Geodynamics,* Cambridge Univ. Press.

Masters, G., Barmine, M. & Kientz, S., 2007. *Mineos User's Manual, Computational Infrastructure for Geodynamics,* Calif. Inst. of Technol., Pasadena, CA.

Métivier, L. & Conrad, C.P., 2008. Body tides of a convecting, laterally heterogeneous, and aspherical Earth, *J. geophys. Res.,* **113**(B11), B11405, doi:10.1029/2007JB005448.

Mitrovica, J.X., Davis, J.L., Mathews, P.M. & Shapiro, I.I., 1994. Determination of tidal h Love number parameters in the diurnal band using an extensive VLBI dataset, *Geophys. Res. Lett.,* **21**(8), 705–708.

Mochizuki, E., 1986. The free oscillations of an anisotropic and heterogeneous Earth, *Geophys. J. Int.,* **86**(1), 167–176.

Nowick, A. & Berry, B., 1972. *Anelastic Relaxation in Crystalline Materials,* Academic Press.

O'Connell, R.J. & Budiansky, B., 1978. Measures of dissipation in viscoelastic media, *Geophys. Res. Lett.,* **5**(1), 5–8.

Park, J. & Gilbert, F., 1986. Coupled free oscillations of an aspherical, dissipative, rotating Earth: Galerkin theory, *J. geophys. Res.,* **91**(B7), 7241–7260.

Petit, G. & Luzum, B. (eds)., 2010. *IERS Conventions,* International Earth Rotation and Reference Service (IERS) Technical Note No. 36.

Qin, C., Zhong, S. & Wahr, J., 2014. A perturbation method and its application: elastic tidal response of a laterally heterogeneous planet, *Geophys. J. Int.,* **199**(2), 631–647.

Resovsky, J.S. & Ritzwoller, M.H., 1995. Constraining odd-degree Earth structure with coupled free-oscillations, *Geophys. Res. Lett.,* **22**(16), 2301–2304.

Ritsema, J., van Heijst, H.J. & Woodhouse, J.H., 1999. Complex shear wave velocity structure imaged beneath Africa and Iceland, *Science,* **286**(5446), 1925–1928.

Shida, T., 1912. *On the Elasticity of the Earth and the Earth's Crust,* Kyoto Imperial University.

Smith, M.L. & Dahlen, F.A., 1981. The period and Q of the Chandler wobble, *Geophys. J. Int.,* **64**(1), 223–281.

Takeuchi, H., 1950. On the Earth tide of the compressible Earth of variable density and elasticity, *EOS, Trans. Am. geophys. Un.,* **31**(5), 651–689.

Thomson, W., 1863. On the rigidity of the Earth, *Phil. Trans. R. Soc. Lond., A.,* **153,** 573–582.

Tromp, J. & Dahlen, F.A., 1990. Summation of the Born series for the normal modes of the Earth, *Geophys. J. Int.,* **100**(3), 527–533.

Tromp, J. & Mitrovica, J.X., 1999. Surface loading of a viscoelastic earth–I. General theory, *Geophys. J. Int.,* **137**(3), 847–855.

Wahr, J.M., 1981a. A normal mode expansion for the forced response of a rotating Earth, *Geophys. J. R. astr. Soc.,* **64**(3), 651–675.

Wahr, J.M., 1981b. Body tides on an elliptical, rotating, elastic and oceanless Earth, *Geophys. J. R. astr. Soc.,* **64**(3), 677–703.

Wahr, J.M. & Bergen, Z., 1986. The effects of mantle anelasticity on nutations, Earth tides, and tidal variations in rotation rate, *Geophys. J. Int.,* **87**(2), 633–668.

Wang, R., 1994. Effect of rotation and ellipticity on Earth tides, *Geophys. J. Int.,* **117**(2), 562–565.

Woodhouse, J., 1988. The calculation of eigenfrequencies and eigenfunctions of the free oscillations of the earth and the sun, in *Seismological Algorithms,* pp. 321–370, ed. Doornbos, D.J., Academic Press.

Woodhouse, J.H., 1980. The coupling and attenuation of nearly resonant multiplets in the Earth's free oscillation spectrum, *Geophys. J. Int.,* **61**(2), 261–283.

Woodhouse, J.H. & Dahlen, F.A., 1978. The effect of a general aspherical perturbation on the free oscillations of the Earth, *Geophys. J. Int.,* **53**(2), 335–354.

Wu, P., 1978. The response of a Maxwell Earth to applied surface mass loads: glacial isostatic adjustment, *Master's thesis,* University of Toronto.

Yuan, L. & Chao, B.F., 2012. Analysis of tidal signals in surface displacement measured by a dense continuous GPS array, *Earth planet. Sci. Lett.,* **355–356,** 255–261.

Yuan, L., Chao, B.F., Ding, X. & Zhong, P., 2013. The tidal displacement field at Earth's surface determined using global GPS observations, *J. geophys. Res.,* **118**(5), 2618–2632.

Yuen, D.A. & Peltier, W.R., 1982. Normal modes of the viscoelastic earth, *Geophys. J. Int.,* **69**(2), 495–526.

Zener, C., 1948. *Elasticity and Anelasticity of Metals,* University of Chicago Press.